Soil Dynamics and Earthquake Engineering 195 (2025) 109431

Contents lists available at ScienceDirect

Soil Dynamics and Earthquake Engineering

journal homepage: www.elsevier.com/locate/soildyn

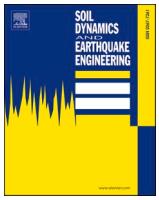

Geotechnical subsoil modelling of a slope from the interpretation of ambient noise measurements and 2D site response analyses

Gaetano Falcone [a,b], Annamaria di Lernia [b,*], Giuseppe Calamita [c], Maria Rosaria Gallipoli [c], Angela Perrone [c], Sabatino Piscitelli [c], Jessica Bellanova [c], Francesco Cafaro [b], Gaetano Elia [b]

[a] Department of Civil, Building and Environmental Engineering (DICEA), Università di Napoli Federico II, Via Claudio 21, 80125, Naples, Italy
[b] Department of Civil, Environmental, Land, Building Engineering and Chemistry (DICATECh), Technical University of Bari, Via Orabona 4, 70125, Bari, Italy
[c] National Research Council of Italy (CNR-IMAA), C.da S. Loja Zona Industriale, PZ, Tito Scalo, Italy

ARTICLE INFO

Keywords:
HVNSR measurements
Buried morphologies
Complex topography
FE numerical modelling
2D site response analyses

ABSTRACT

Within the context of seismic risk assessment, the prediction of the dynamic response of natural slopes is strictly related to the accurate definition of the geotechnical subsoil model. This aspect is particularly challenging for those slopes characterised by the presence of buried morphologies, for which the vertical and lateral heterogeneities of the subsoil setting may predispose them to additional risks during seismic events. The paper proposes a methodological procedure aimed at identifying preliminary subsoil models of areas characterised by uneven topography and buried lithological bodies of uncertain morphology, through the comparison of parametric site response analyses and site-specific geophysical surveys. The procedure, tested with reference to the prototype case study of Costa del Canneto slope in Southern Italy, proves to be a useful tool to reduce the uncertainties associated with the presence of complex subsoil settings, including potential buried morphologies. Indeed, over several geotechnical models tested, the numerical analyses provide amplification profiles of the fundamental frequency reasonably comparable with data from ambient vibration measurements only for few of them. This allows to restrict the number of possible slope models and can be used to guide the design of additional in-situ geotechnical investigations needed to better characterise the stratigraphy of the area and constrain the geometry of the expected buried morphologies.

1. Introduction

In the framework of seismic risk assessment, the prediction of the ground response over a large area is one of the key steps for the emergency management after important events and the development of reliable risk mitigation strategies [1–5]. The accurate evaluation of the seismic site response is strictly related to the proper reconstruction of the geotechnical subsoil model, defined in terms of morphology of the stratigraphic contacts, location of the seismic bedrock, dynamic properties of the soils and succession of soil layers. Within this context, natural slopes characterised by buried lithological bodies of uncertain morphology represent a challenging scenario for the seismic response assessment, as their vertical and lateral heterogeneities predispose them to additional risks during seismic events with respect to the case of homogeneous deposits with an uneven ground surface [6–11].

When dealing with sites for which the subsoil setting is not well-characterised, the adoption of non-invasive and expeditive site investigations could be useful for a first definition of preliminary geotechnical subsoil models, in order to reduce the degrees of uncertainty and successively address a more detailed investigation. Among the available surface site tests, seismic ambient noise measurements, obtained through the Horizontal-to-Vertical Noise Spectral Ratio technique (HVNSR), are those extensively employed for various purposes, including large-area applications such as seismic microzonation, as well as the investigation of local site conditions. For instance, HVNSR measurements supported by available geological data are used in microzonation studies to recognise areas characterised by the same seismic behaviour during earthquakes, without conducting deep site-specific

* Corresponding author.
E-mail addresses: gaetano.falcone@unina.it (G. Falcone), annamaria.dilernia@poliba.it (A. di Lernia), giuseppe.calamita@cnr.it (G. Calamita), mariarosaria.gallipoli@cnr.it (M.R. Gallipoli), angela.perrone@cnr.it (A. Perrone), sabatino.piscitelli@cnr.it (S. Piscitelli), jessica.bellanova@cnr.it (J. Bellanova), francesco.cafaro@poliba.it (F. Cafaro), gaetano.elia@poliba.it (G. Elia).

https://doi.org/10.1016/j.soildyn.2025.109431
Received 15 November 2024; Received in revised form 25 February 2025; Accepted 3 April 2025
Available online 13 April 2025

investigations [12–14]. In other applications, the ambient noise vibration measurements are adopted as an effective tool to obtain a first-glance interpretation of the geological models [15–17]. In these cases, a first indication about the depth of the seismic bedrock is provided by the relationship between the fundamental frequency determined from HVNSR data and the depth of the main impedance contrast of the deposit. As an example, the work by Albarello et al. [17] proposes a ready-to-use table to rapidly identify the depth of the rigid bedrock as a function of the resonance frequency of the HVNSR data.

Moreover, seismic ambient noise measurements are widely adopted to highlight site effects induced by complex subsoil and topographic settings characterised by stratigraphic heterogeneity [18–23]. For example, in the work by Diaz-Segura [18] systematic microtremor testing was conducted to determine the dynamic response of sites located in the Fenwei Basin (China) characterised by complex stratigraphic conditions. While the above-mentioned studies focused on the effect of subsoil setting on seismic amplification, HVNSR data can also be used to study the directivity of ground motion induced by uneven topography or by a buried morphology, such as a sediment-filled valley or a sliding body characterised by softer soils [24–32]. In the work by Mele et al. [33], the HVNSR passive seismic technique was adopted to identify the shape of a buried valley in the Italian Central Alps, revealing that the morphology of that area is controlled by an active deep-seated gravitational slope deformation. In the study by Pazzi et al. [34], the seismic noise measurements allowed to identify abrupt changes in seismic impedance related to the presence of landslide boundaries, affecting both the shear wave velocity and the density of the soils. In other studies, the ambient noise measurements are adopted in combination to other geophysical tests for the identification of landslide-prone areas [35,36]. For example, in the work by Innocenti et al. [37] the geophysical techniques and the ground penetrating radar measurements were adopted to support the geotechnical investigations, in order to identify a reliable geotechnical model to be implemented in the numerical modelling. In the study by Calamita et al. [38], the integration of in-situ geoelectrical and seismic methods together with satellite data was adopted to characterise a portion of an urban area affected by ground instability phenomena. The results from geoelectrical and seismic methods were interpreted with the support of stratigraphic data to reconstruct the geometry of the subsoil.

Several scientific studies have underlined the importance of using information retrieved from ambient noise measurements, geophysical surveys and 1D site response analyses for the construction of reliable models of soil deposits characterised by the presence of a high impedance contrast [17,39–43]. In the work by Diaz-Segura [44], the fundamental frequency of vibration of sloping areas was estimated by means of 2D and 3D finite element analyses and HVNSR measurements, showing a good agreement between the two approaches. Giallini et al. [45], instead, showed that the outcomes of seismic ambient noise measurements, appropriately interpreted and supported by the results of preliminary 2D numerical simulations, may provide an indication of a possible contrast of impedance between soil layers. In this work, the subsoil model was defined on the basis of comprehensive site surveys, including in-depth site investigations, while the 2D numerical seismic site response analyses along two selected sections were compared to HVNSR data along the intersection vertical in terms of fundamental frequency of the soil deposit.

Recently, based on a parametric numerical investigation on ideal slope models, Falcone et al. [46] demonstrated that the presence of either a shear band confining a landslide body or, more generally, a subsoil buried morphology represents an impedance contrast strongly affecting the seismic response, not only in terms of resonance frequency, but also in terms of seismic amplification at the ground surface. Indeed, the numerical results gave evidence to the complex interaction between the inclination of the slope, the thickness and morphology of the shear band and the slope amplification response, affecting the distribution of the amplification along the slope.

Inspired by these numerical findings on ideal cases, this paper proposes a relatively simple and expeditive methodological procedure to develop reliable geotechnical subsoil models, based on the joint interpretation of non-invasive geophysical investigations and parametric 2D numerical analyses of the seismic site response. Starting from the geological, geomorphological and geotechnical information retrieved from the available historical archives, plausible geotechnical subsoil models could be constructed by comparing the ambient noise measurements and the results of dynamic simulations performed with reference to different 2D subsoil models, built on the basis of the available information and iteratively adjusted to get results compatible with the HVNSR data. The proposed procedure has been tested with reference to a prototype area, the Costa del Canneto slope (Ferrandina, Matera, Italy), characterised by uneven topography and complex subsoil setting, potentially including lithological bodies causing geological and geomechanical heterogeneity [47–49]. The selected area belongs to the mountain area of the Basilicata Region (Southern Italy), prone to landslides and affected by high seismic hazard. It is one of the sites under investigation within the MITIGO project (https://www.mitigoinbasilicata.it/), which aims at providing strategies for the mitigation of hydrogeological and seismic risks for structures and infrastructures. The main novelty of the work lies in the extensive adoption of HVNSR data in combination with parametric 2D numerical simulations for the definition of the most realistic subsoil model of a real slope with buried morphologies, for which few geological and geotechnical information are available. The proposed procedure serves as a foundation for a cost-effective and less invasive approach to design in-depth site investigations specifically tailored for the targeted area of interest. More generally, the outcomes of this research can provide engineers, planners, and decision-makers with valuable tools and guidelines to reduce uncertainties associated with the geotechnical and geomorphological study of slopes, characterised by complex subsoil settings including potential buried morphologies.

2. Proposed methodological approach

The proposed methodological approach, synthesised in the workflow shown in Fig. 1, is intended to provide a cost-effective tool for the definition of the subsoil model for slopes characterised by complex settings, capable of reducing uncertainties associated with the geotechnical and geomorphological study and guiding the design of in-depth site investigations.

The first stage of the procedure requires the geological and geomorphological analysis of the area, leading to a preliminary identification of the possible buried morphology. The second step involves the collection of soil data, *i.e.* physical and mechanical properties, retrieved from both historical archives and literature. Then, Step 3 concerns the parametrization of the subsoil setting, requiring the definition of preliminary site models with vertical and/or lateral heterogeneity, possibly including a buried morphology, based on the observations of the first two steps. The fourth and fifth stages are divided into two sub-steps, involving the execution and interpretation of seismic ambient noise measurements (sub-steps 4a and 5a) and the execution and interpretation of numerical simulations of the seismic slope response using very weak input motions (sub-steps 4b and 5b), in order to compare the results from the 2D site response analyses with the HVNSR data. As well-recognised in the scientific literature (see, for example, [17,50]), the HVNSR measurements are deemed to be related to the results of seismic site response analyses in terms of resonance frequencies of the subsoil deposit. Indeed, the frequency corresponding to the maximum value of the ratio of the horizontal to vertical (H/V) spectral components of ambient vibrations has a strict correspondence with the local resonance frequency of the soil deposit, which could be determined through numerical simulations as the ratio between the horizontal response at the ground surface and the horizontal component of the motion at the soil-bedrock interface. Nevertheless, the HVNSR measurements and

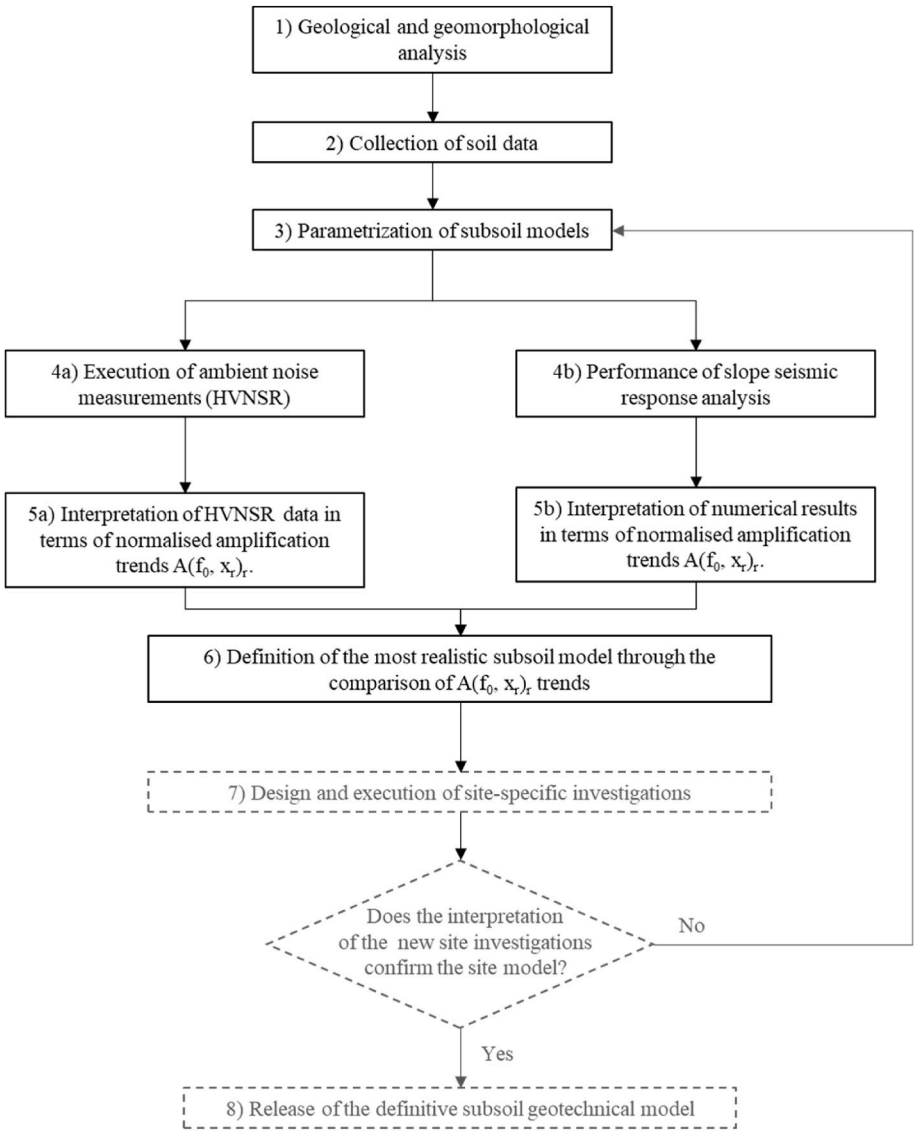

Fig. 1. Workflow for the definition of a reliable subsoil model based on parametric numerical analyses of the seismic slope response and seismic ambient noise measurements. Steps in grey have not been completed for the selected case study.

numerical results are not directly comparable in terms of seismic amplification amplitudes. Therefore, to easily and qualitatively compare these data, the interpretation of in-situ and numerical results should be carried out by normalizing the amplification amplitude at the fundamental frequency f_0 obtained at different locations by its maximum value attained along the slope. Thus, the normalised amplification $A(f_0, x_r)_r$ has been defined in Eq. (1) as the ratio of the seismic amplification $A(f_0, x_r)$ at a specific relative distance x_r (Eq. (2)) and the maximum value of $A(f_0, x_r)$ along the slope:

$$A(f_0, x_r)_r = \frac{A(f_0, x_r)}{m\,a\,x\left[A(f_0, x_r), 0 \le x_r \le 1\right]} \quad (1)$$

$$x_r = \frac{x - x_{0,slope}}{L_{slope}} \quad (2)$$

The seismic amplification $A(f_0, x_r)$ can be obtained as the ratio between the Fourier spectrum at the ground surface and the Fourier spectrum at the soil-bedrock interface in correspondence of the fundamental frequency of the system, f_0, while x is the abscissa of the point of interest, $x_{0,slope}$ is the abscissa of the slope crest and L_{slope} is the length of the slope (Fig. 2). In the case of real, more complex topographic

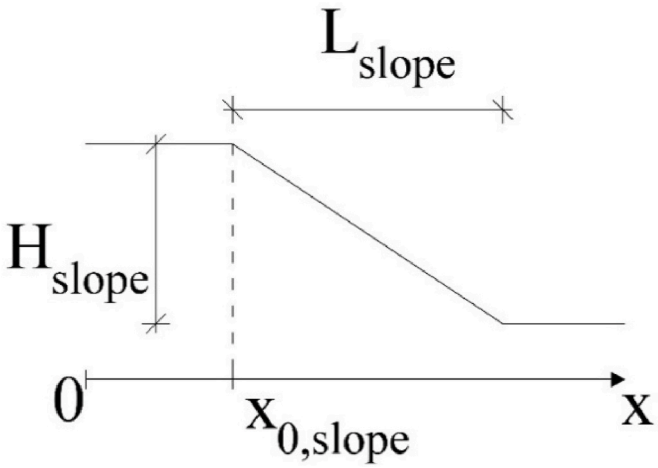

Fig. 2. Schematic representation of the slope.

geometries, the definition of the height H_{slope} and the length L_{slope} of the slope depends on the extension of the investigated area of interest and should be based on engineering judgement.

In order to make the proposed methodology as general as possible, the relative distance x_r is adopted in the interpretation of in-situ measurements and numerical simulations. The relative distance x_r is useful when the results of different slopes need to be compared; if a single slope is analysed (as in the case of the present paper), the normalization of the

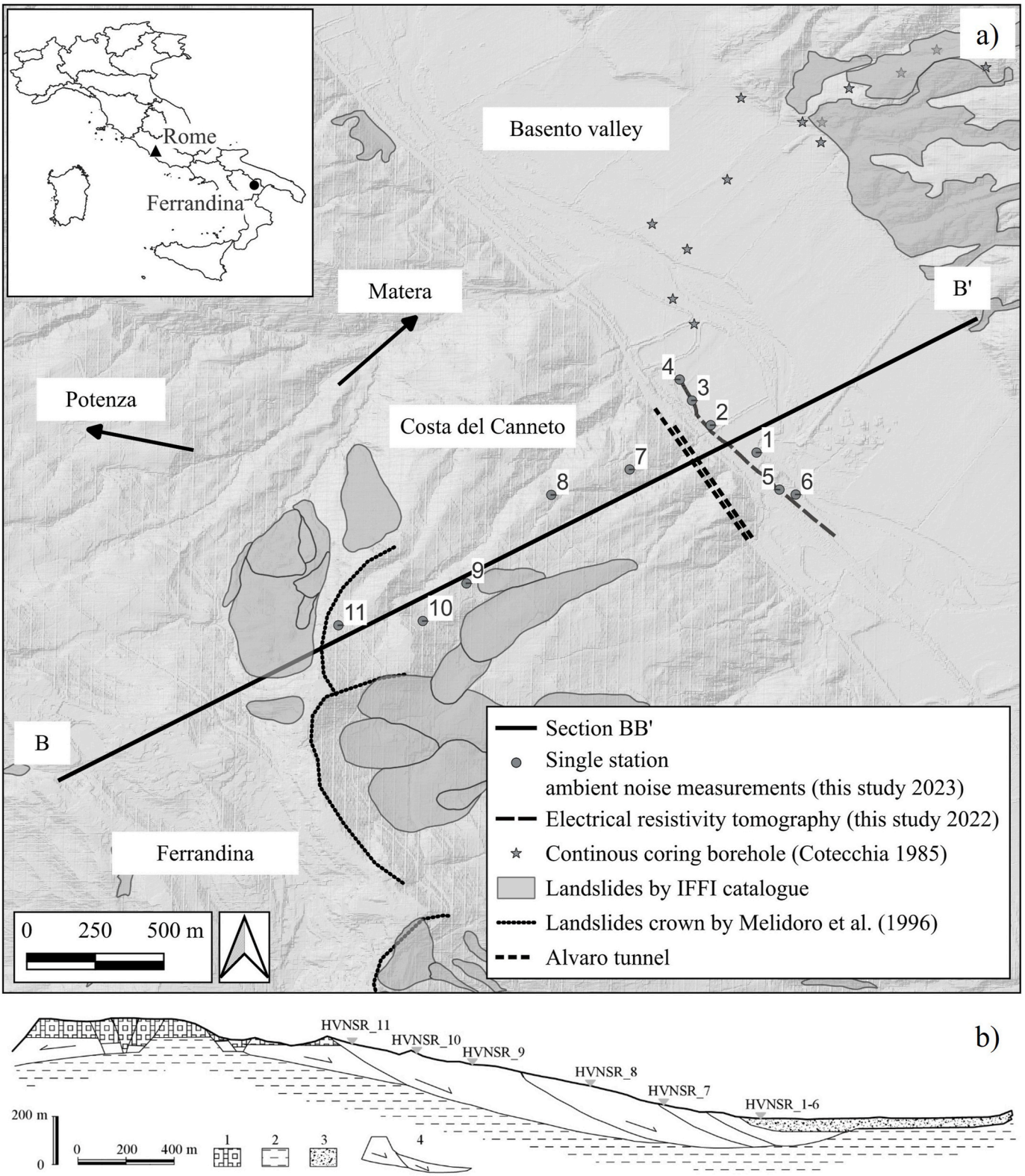

Fig. 3. (a) Map of the investigated area showing the location of the past and recent in-situ investigations and the landslide borders identified by Melidoro et al. [48] and mapped in the IFFI catalogue [51]; (b) geological section BB' (modified after Melidoro et al. [48]) with the location of the single station ambient noise measurements. In the figure: 1) sand and conglomerate, 2) blue-grey clay, 3) alluvial material, 4) sliding body.

distance is not strictly necessary.

It should be remarked that a continuous profile of the normalised amplification $A(f_0, x_r)_r$ could be retrieved from the numerical simulations by selecting a large number of sampling points on the model surface with a small distance, depending on the degree of accuracy the user would like to achieve. Conversely, the distribution of the normalised amplification $A(f_0, x_r)_r$ retrieved from HVNSR data is discrete, since a smaller number of measurements is typically performed in-situ. In general, the higher is the number of in-situ HVNSR measurements, the more accurate is the comparison with the numerical results.

Stage 6 requires the comparison of field data and numerical analyses results, elaborated in terms of amplification distribution along the slope surface, aimed at selecting the most realistic subsoil models. Once the possible subsoil geotechnical models are identified, these should be verified and refined in Step 7 through the design and execution of site-specific investigations (*e.g.*, continuous coring boreholes, inclinometers, piezometers, down-hole tests, etc.). If the detailed site investigations confirm one of the proposed models, then the last Step 8 could be pursued through the release of the definitive subsoil geotechnical model of the site of interest. It is evident that the proposed procedure is iterative, as the subsoil model parametrization could be repeated several times to achieve the best fitting between numerical results and HVNSR measurements.

In the present work, the proposed methodological approach has been adopted to define several possible geotechnical models for the prototype slope in the Costa del Canneto area, located in the Basilicata region within the Italian Southern Apennines (Fig. 3). The Ferrandina urban area stands at the top of the Costa del Canneto slope, while at its toe the slope is crossed by the Alvaro tunnel on the Basentana State Road, running parallel to the Basento River (Fig. 3a). The site has been selected as representative of those areas characterised by uneven topographic conditions and complex subsoil settings, potentially including buried morphologies due to the presence of landslides, also interacting with an underground infrastructure (Fig. 3b).

The application of the procedure to the selected case study has started from the collection of geological and geomorphological data (Step 1), retrieved from national datasets [51] and the literature [47,48,52], and the collection of physical and mechanical soil parameters (Step 2), derived from previous site investigations, including continuous boreholes, seismic refraction, geoelectrical surveys (Fig. 3), as deduced from the available literature [47–49,53,54]. These two steps have led to a preliminary definition of several geotechnical slope models.

Since only few site data are available, a great effort in the parametrization of the slope models has been made to include the largest number of possible and suitable 2D models (Step 3). These have been defined neglecting the presence of the Alvaro tunnel and accounting for different subsoil conditions (including homogeneous and heterogeneous cases in terms of stratigraphy), several configurations of the buried morphologies, but also different topographic settings. The execution and analysis of HVNSR measurements (Steps 4a and 5a) has provided a benchmark for the interpretation of the numerical results of the preliminary 2D subsoil models (Steps 4b and 5b). Also, the results of the electrical resistivity tomography (ERT) executed in the same area (Fig. 3) have been adopted to support the selection of the 2D subsoil models. A total number of 11 single-station seismic surveys have been carried out, 6 along the ERT profile and 5 along the BB' section of the slope (Fig. 3), with different distances between each location.

The seismic ambient vibration registrations have been acquired through a digital three-component velocimeter "Tromino" (Micromed-MoHo s.r.l.) with a 128 Hz sampling frequency and analysed with the software Grilla, by applying the HVNSR technique [50,55] in the frequency range 0.1–20 Hz, following the SESAME recommendations [56]. In accordance with these guidelines, the three orthogonal components of the 20-min-long recordings have been divided into 50 s non-overlapping windows, which correspond to at least ten times the soil fundamental period (~0.2–0.3 Hz, *i.e.* ~ 3–5 s). A longer window length was not feasible, as it would have resulted in an insufficient number of windows for a stable statistical analysis [57]. Each windowed signal has been pre-processed (detrended, tapered with a Bartlett window, zero-padded), filtered in the time domain by the STA/LTA (Short Time Average/Long Time Average) algorithm before being Fast Fourier-transformed. The ratio between the geometric mean of the horizontal component and the vertical one has been calculated for each window, and the average and standard deviation have been then obtained for all the windows.

The electrical resistivity test has been conducted along a 940 m profile located at the base of the slope, between the Alvaro tunnel and the Basento River (Fig. 3), using a Syscal Pro (IRIS Instr.) connected to multi-electrode cables with 48 electrodes spaced 20 m apart. Apparent resistivity data have been collected with a Wenner-Schlumberger electrode array and then inverted to obtain the electrical resistivity model [58]. Given the data quality and expected subsoil variations, a L2 norm has been applied to both the data misfit and model smoothness in the optimisation function [59].

The 2D subsoil models have been implemented in the FE code PLAXIS 2D [60] to perform time-domain dynamic simulations by applying weak Ricker wavelets as reference motion. Different constitutive models of increasing complexity, *i.e.* the linear visco-elastic and the hardening soil model with small strain stiffness HSsmall [61,62] models, have been adopted to describe the behaviour of the slope soils, whose geotechnical properties have been retrieved from the available literature [47,48,53,54]. Significant attention has been given to the definition of the soil small-strain shear stiffness, G_0, fundamental for the accurate evaluation of the seismic site response. Given the lack of site-specific geotechnical investigations for the dynamic characterisation of soils, three different shear wave velocity profiles have been selected representing the behaviour of the soils encountered in the area, as better described in the next section. The output of the numerical simulations has been retrieved with reference to sampling points selected on the surface of each model with a distance of 50 m.

The process of parametrization has been repeated to refine the preliminary subsoil models, until the numerical results become compatible with the HVNSR data. After performing a set of 20 numerical analyses with 20 different subsoil models, three reliable geotechnical models of the slope, also incorporating buried morphologies, have been identified (Step 6). Thus, the proposed approach has been applied up to Stage 6 for the selected case study, but the identified slope models can now guide site-specific geotechnical investigations to validate or confute the assumed subsoil models.

3. Application of the proposed methodology to the prototype slope

3.1. Geology and geomorphology of the prototype slope

From a geological point of view, the Costa del Canneto area lies within the Bradanic Foredeep [48]. Given the lack of geognostic investigations directly executed in this specific area, the geological and geomorphological analyses have been based on available literature data. In particular, the geological (and geotechnical) analysis has been carried out considering the results of the geognostic campaign conducted in 1985 for the design of a railway line from Ferrandina to Matera [47], in an area located at north-east of the Basento River (Fig. 3) on the left side of its valley (*i.e.*, opposite to the slope of interest). The 1985 geognostic campaign consisted of 55 vertical continuous boreholes, from which more than 100 undisturbed soil samples were retrieved, inclinometers, 30 seismic refraction profiles and 30 geoelectrical surveys. Based on the interpretation of these boreholes, Cotecchia [47] deduced two stratigraphic schemes: the first one, referring to both the right and left side of the Basento valley, is characterised by a 5–15 m thick shallow layer of yellow clay, overlying a blue-grey clay layer; the second stratigraphic scheme, pertaining to the Basento valley, is characterised by a first layer

of alluvial deposits, 4–9 m thick, underlain by the blue-grey clay layer. The blue-grey clay stratum could reach a thickness of about 500 m [63] and can be interlayered by very thin sand strata.

Consistently with the subsoil models provided by Cotecchia [47], the area of interest might be considered as formed by a sedimentary sequence (middle-low Pleistocene) in the upper part, consisting of open-shelf muddy deposits, named in the literature as Sub-Apennine Clays and recalled herein as blue-grey clays, and by a shallow layer of conglomeratic sand (Fig. 3a). The blue-grey clays are characterised by very thin layers of sand or silt. The shallow part of the blue-grey clays, generally 20–30 m thick, is made of the so-called yellow clays, which are the results of weathering or, in general, alteration processes [47,53]. Moreover, the Ferrandina urban area lies on an alluvium layer, made by sands, silty sands and coastal conglomerates with a maximum thickness of 90 m (Fig. 3b).

The entire area of interest is characterised by steep slopes with ground surface inclination higher than 50% and it is expected to be affected by both seismic topographic amplification and slope failures. Indeed, deep slope instability phenomena are recognised in the Ferrandina area, as shown in Fig. 3a, where the landslides retrieved from the IFFI Italian catalogue [51] based on site surveys and the geomorphological reconstruction proposed by Melidoro et al. [48] are mapped. Cotecchia [47] also identified potential sliding bodies composed of remoulded clays in the region crossed by the Ferrandina-Matera railway, by analysing the vertical profiles of physical and mechanical soil parameters and the inclinometric data. The maximum depth of the sliding surfaces recognised by Cotecchia [47] on the left side of the Basento River valley varies between 30 and 80 m, while the geomorphological study shown in Melidoro et al. [48] suggested a sliding body more than 100 m deep for the area of interest on the right side of the valley. Although the analysis and the diagnosis of the failure mechanisms affecting the slope is beyond the scope of this study, it can be inferred that the presence of buried morphologies in the investigated area is plausible, and it represents the starting point for the parametric analyses carried out to suggest reliable subsoil models of the slope.

3.2. Geotechnical properties of the slope soils

According to the geological analysis, the Costa del Canneto area is mainly characterised by outcropping formations of yellow clay, blue-grey clay, and alluvial deposits of the Basento River. The mechanical properties of the slope soils have been retrieved from previous geotechnical investigations conducted in the area close to Costa del Canneto slope [47,48,52,54]. Concerning the blue-grey clay, the unit weight varies from 18 kN/m^3 to 21 kN/m^3, the effective cohesion, c', ranges from 15 kPa to 30 kPa, the effective friction angle, φ', encompasses the interval of 17–25°, the Plasticity Index, PI, ranges between 15% and 30%, while the overconsolidation ratio, R_0, is in the range 1.8–2.7.

Since no experimental data are, instead, available to characterise the dynamic properties of the Costa del Canneto slope soils, the yellow and the blue-grey clays have been assumed to behave at very low shear strains (γ < 1E-6%) similarly to the Montemesola clay (Taranto, Italy) [53], characterised by a PI equal to 26%, analogous to that pertaining to the clayey soils found in the area of interest. Considering the Montemesola clay, an empirical relationship to evaluate the variation of G_0 as a function of the soil composition, the mean effective stress state p', the overconsolidation ratio R_0 and the stress sensitivity S_σ was proposed in the work by Cafaro and Cotecchia [53]. In the present work, the relationship has been slightly modified as shown in Eq. (3), in order to be consistent with the Viggiani and Atkinson equation [64], for which the parameter A* should be equal to 1250 for reconstituted clays ($S_\sigma = 1$) with PI = 26 %. The coefficients a and b equal to 3.0969 and 0.1834, respectively, have been obtained through the best fitting of the available data (see Cafaro and Cotecchia [53] for more details) in terms of (A*, S_σ) pairs. Moreover, m* and n* are set equal to 0.225 and 0.78, respectively, based on the correlation with PI provided by Viggiani and Atkinson [64] for PI = 26 %.

$$\begin{cases} G_0(z) = A^* \cdot p'^{n^*} \cdot R_0^{m^*} \\ A^* = 10^{a \cdot e^{Log(S_\sigma) \cdot b}} \end{cases} \quad (3)$$

Fig. 4 illustrates the shear wave velocity profiles with depth, $V_S(z) = [G_0(z)/(\gamma/9.81)]^{0.5}$, estimated through Eq. (3) for the blue-grey, yellow, and reconstituted clays, assuming S_σ equal to 2.4, 1.5, and 1.0, respectively, and R_0 equal to 2.0, 2.5 and 1.0, respectively. It is straightforward to recognise that at the same p' value, the blue-grey clay is stiffer than the yellow clay, which in turn is stiffer than the reconstituted clay. In the same figure, the range of V_S provided by Romagnoli et al. [65] for middle-low plasticity clay is also shown with a shaded area. The profiles selected for this study fit well with the shaded area, especially for depths lower than 85 m, which is the maximum depth of the in-situ surveys analysed by Romagnoli and co-workers [65].

In the following, the blue-grey, yellow and reconstituted clays are referred to as Soil_1, Soil_2 and Soil_3, in order to identify three materials characterised by different shear stiffness profiles with depth, representing, in general, an intact soil, a weathered soil and a remoulded soil, respectively. Such geotechnical characterisation is only an attempt to provide reference data for the soils of interest, but a proper in-situ dynamic campaign should be carried out with the aim of reducing uncertainties and establishing a reliable geotechnical model for the examined area.

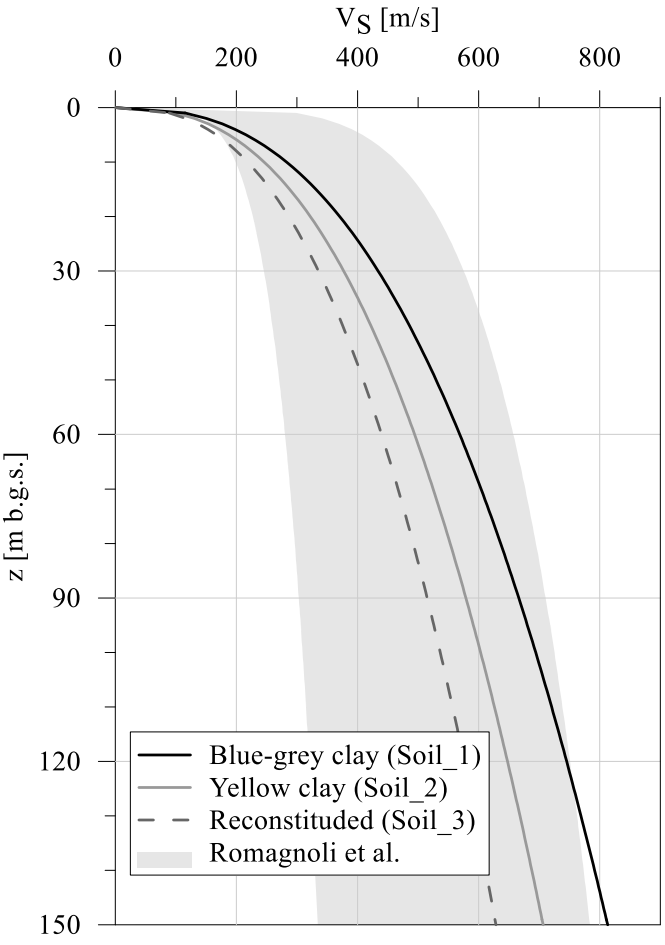

Fig. 4. Reference $V_S(z)$ profiles for the blue-grey, yellow and reconstituted clays. The shaded area refers to the range of V_S provided by Romagnoli et al. [65].

3.3. Execution and interpretation of geophysical surveys

As already discussed in the methodological section, in-situ geophysical surveys have been carried out in October 2022 and July 2023 along a section crossing longitudinally the slope and a section crossing transversally its toe (Fig. 3). More specifically, six single-station seismic surveys have been carried out along the ERT section located downslope of Costa del Canneto, while five single-station ambient noise measurements have been executed along the BB' section, crossing the tunnel in the proximity of the toe (Fig. 3). These geophysical surveys served to better delineate the expected subsurface lithological bodies and guided the stage of the subsoil model parametrization.

Fig. 5 illustrates the ERT profile and the HVNSR curves resulting from the ambient noise measurements elaboration along the same section, together with the geo-lithological section along the Alvaro tunnel proposed in the literature [48]. It should be mentioned that the ERT section runs almost parallel to the Alvaro tunnel at a distance of approximately 150–200 m.

The ERT (Fig. 5b) shows a ~25 m thick layer of relatively more resistive material (resistivity $\rho > 48$ Ωm) resting on a more conductive soil. The shallow resistive layer shows a more regular shape in the SE part of the ERT than in the NW part. In the latter, starting from 640 m along the profile, the resistive layer seems to deepen and expand. The underlying more conductive material, which occupies almost the entire ERT section, is characterized by a layered structure reaching a maximum depth of ~120 m, particularly in the SE part of the section. As well as for the shallow resistive layer, the conductive material shows a more irregular distribution in the NW portion of the ERT. The resistivity model highlights the presence of evident vertical discontinuities at ~140 m and ~480 m from the origin of the profile.

The comparison of the ERT profile to the geological-geomorphological section along the Alvaro tunnel (Fig. 5a) suggests that the slope in the vicinity of the tunnel is affected by complex phenomena characterised by multiple reactivations, involving multiple sliding surfaces and the presence of vertical infill channels. The deepest sliding surface is placed at about 120 m, in good agreement with the depth of the electrical resistivity discontinuity between the conductive layer and the underlying relatively more resistive soil. Furthermore, the vertical filling channels in the section can help to explain the vertical resistivity discontinuities shown by the ERT.

The average HVNSR curves obtained for the recordings close to the NW part of the ERT (HVNSR #1–HVNSR #4, Fig. 5e–h) generally do not exhibit well-defined resonance peaks. While some amplifications are observed, the fact that the uncertainty band of the mean H/V curve reaches amplitude values just below 2 indicates that further verification is needed. Only for HVNSR #1 the average H/V curve (Fig. 5e) shows amplitude values greater than 2 within a frequency range of approximately 1–3 Hz, which could suggest the presence of a significant impedance contrast [56]. The results obtained close to the SE part of the ERT (HVNSR #5 and HVNSR #6) show mean H/V ratios significantly greater than 2 for frequencies between 0.2 Hz and 0.3 Hz and between 10 and 20 Hz (Fig. 5c and d). This suggests the presence of strong impedance contrasts, likely due to a soft sediment layer overlying a much stiffer material. A common feature of all the HVNSRs along the ERT profile is the de-amplification (*i.e.*, $A < 1$) occurring between 5 and 10 Hz, which is typically associated with the inversion of shear wave velocity due to the presence of a softer layer beneath a stiffer one [66]. Although mechanical and electrical properties are not directly

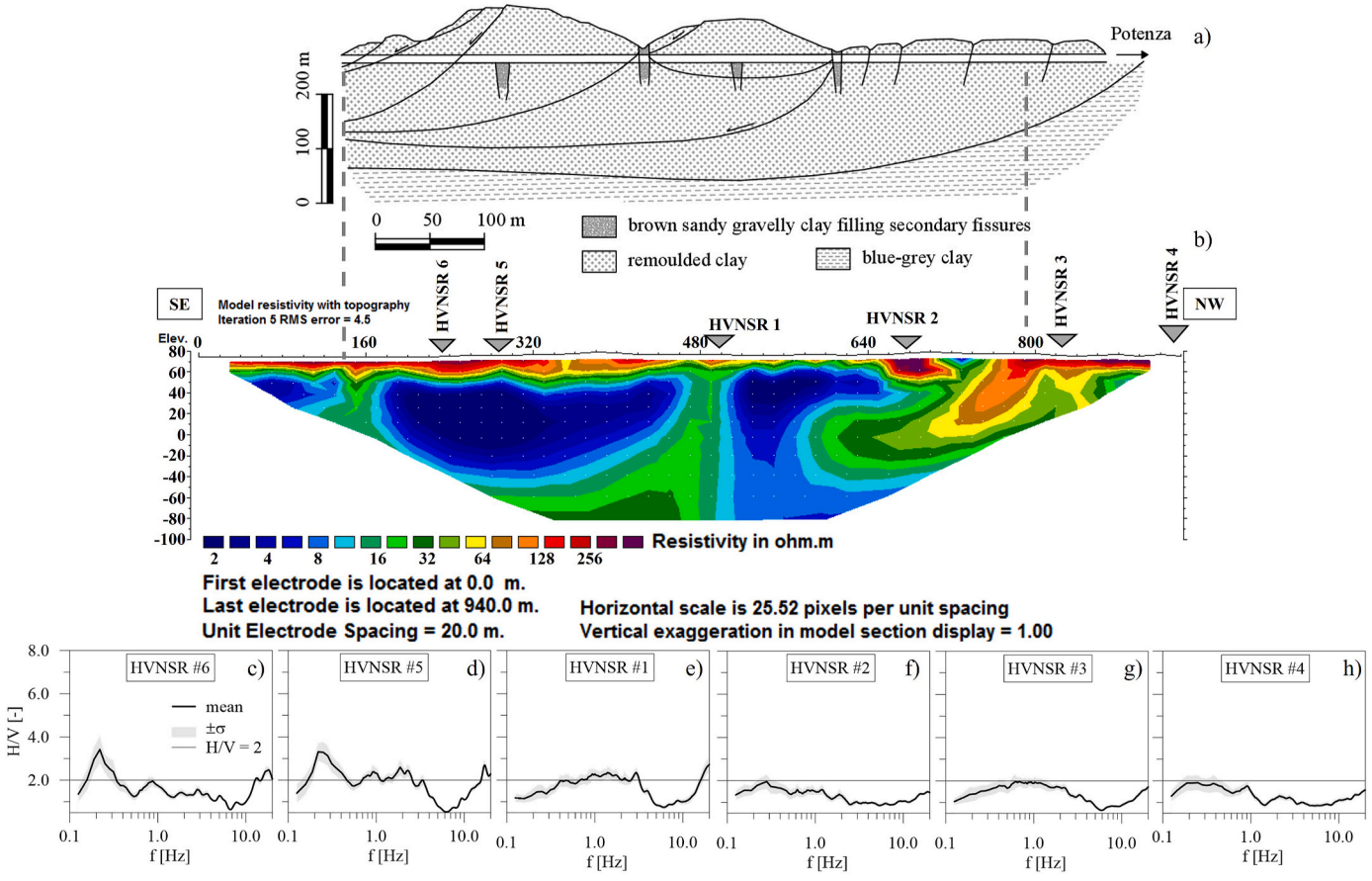

Fig. 5. (a) Geo-lithological section, presented in Ref. [48], along the Alvaro tunnel and (b) electrical resistivity tomography ERT section, located downslope the Alvaro tunnel, reporting the projection of the single station ambient noise locations (section traces are located as shown in Fig. 3a); (c–h) HVNSR curves resulting from the ambient noise measurements elaboration along the ERT. Note that figures a) and b) are not in scale.

correlated, it could be assumed that the material with higher electrical conductivity highlighted by the ERT consists of less compact material resting on a more resistive and stiffer soil.

Low-frequency HVNSR peaks are attributable to mechanical impedance contrasts between cover materials and the seismic bedrock. Assuming a one-dimensional (1D) model of the subsurface with shear wave velocity values increasing with depth and approximating Vs values with the $V_{S,30}$ values ~270–550 m/s on average, as suggested in Mori et al. [67], such low-frequency peaks (0.2–0.3 Hz) are generated at depths greater than about 200 m. The higher-frequency peaks (10–20 Hz) are, instead, likely caused by very shallow (a few meters, at maximum) mechanical impedance contrasts.

The results of the ambient noise measurements executed along the longitudinal section BB' are illustrated in Fig. 6, together with their location along the slope section. Similar to the HVNSR #5 and HVNSR #6 results, the HVNSR curves obtained from the measurements taken along the slope (HVNSR #7–HVNSR #11) highlight amplitudes significantly greater than 2 at frequencies around 0.2–0.3 Hz (Fig. 6b–g). The persistence of the amplification frequency in the measurements taken at different points in the area suggests that it is a site-specific characteristic and that the site is characterised by a very deep mechanical impedance contrast. The reliability of these peaks at relatively low frequencies was confirmed by the presence of the typical characteristic pattern observed in the Fourier spectra of the individual components, where the amplitude of the vertical component is reduced over a limited bandwidth compared to the amplitudes of the horizontal spectra. In some cases, values of H/V ratios barely greater than 2 are present both at low frequencies, *i.e.*, <1 Hz, for HVNSR #10 and HVNSR #11, and at higher frequencies, for HVNSR #7 and HVNSR #11, linked to contrasts in mechanical properties between different materials within the deposit. The shapes of the H/V curves at these frequencies shows multiple closely spaced peaks or broadened, not well defined, peaks with the presence of shoulders and humps, generally indicative of lateral variability of subsurface properties and conditions that deviate from the 1D condition [68].

According to the Step 5a of the methodology, the HVNSR measurements should be interpreted in terms of distribution of $A(f_0, x_r)_r$ along the investigated sections. Given that the ambient noise measurements along the ERT section, characterised by a slight amplification, proved the indication of possible buried morphologies in the SE portion, only the HVNSR data along the longitudinal slope section BB' have been examined in detail, since the reconstruction of the subsoil conditions along the sloping area is of greater interest. It should be mentioned that the proposed methodology might also be applied to flat areas, where complex subsoil conditions might be detected.

To assess whether a buried morphology, or more generally, a complex subsoil setting should be expected for the area of interest, the $A(f_0, x_r)_r$ profile retrieved from HVNSR data has been compared to the $A(f_0, x_r)_r$ profile obtained through the parametric numerical simulations performed on the ideal cases presented by Falcone et al. [46] and illustrated in Fig. 7 for the relative distance x_r between 0 and 1. The numerical investigation consisted in performing two sets of 2D dynamic analyses with reference to steep (*i.e.*, inclination of 22°) and gentle (*i.e.*, inclination of 5°) slope models, each including a shear band characterised by different thickness ratios, H_{sb}/H_{slope} (where H_{slope} is the height of the slope and H_{sb} is the thickness of the shear band) ranging between 2.5% and 20%. The normalised amplification profiles $A(f_0, x_r)_r$ of the ideal slope models were evaluated for different points on the ground surface (with a spatial step of 25 m), by estimating the amplitude of the amplification function at the fundamental frequency f_0, depending on the model geometry and soil characteristics. Therefore, for the steep slopes the f_0 values range between 2 and 2.5 Hz, while for the gentle slope case the fundamental frequency assumes values between 1 and 1.25 Hz. The distribution of the normalised maximum amplification at the ground surface revealed to be strongly related to the slope inclination (Fig. 7). In particular, for steep slopes the highest seismic amplifications are concentrated in the upper portion and tend to reduce toward the toe of the slope, independently on the shear band thickness. Conversely, for gentle slopes the amplification profiles are characterised by oscillations around high values along the whole slope surface with

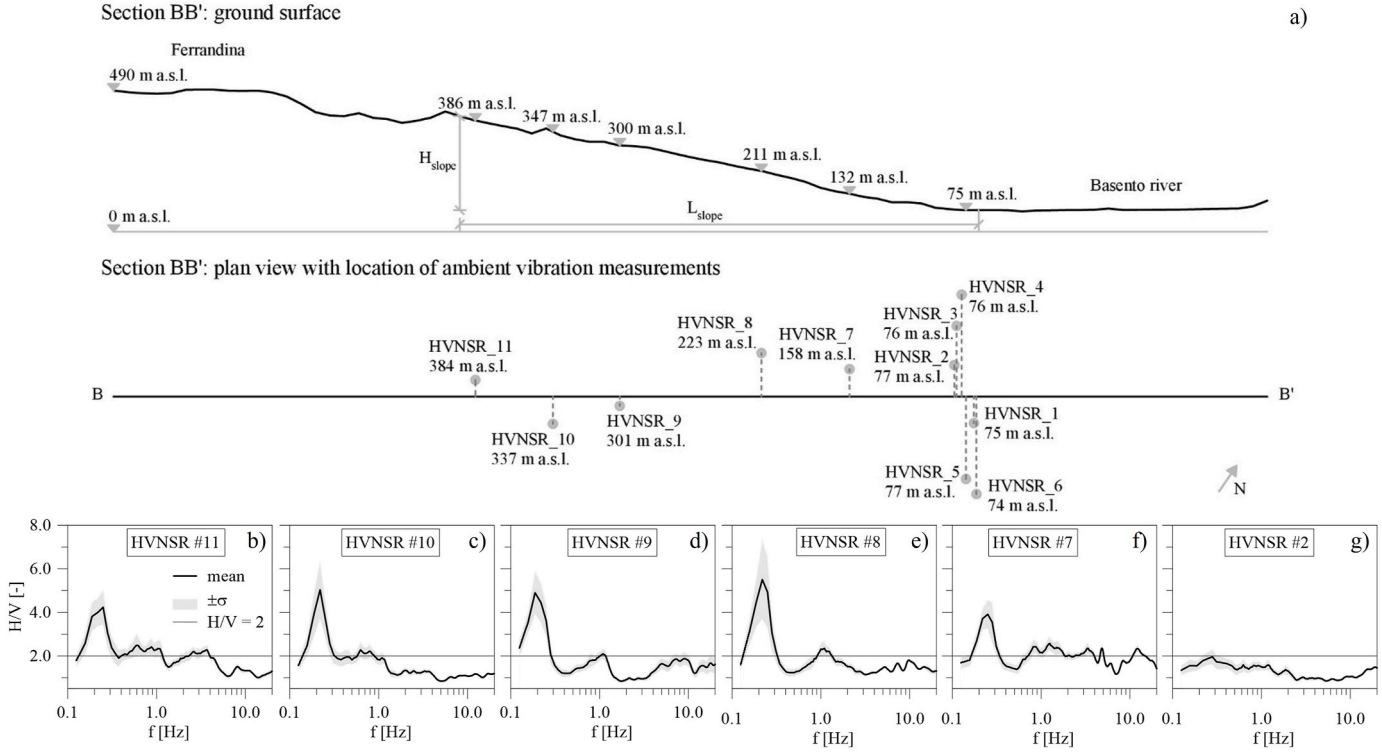

Fig. 6. (a) Profile of the section BB' (ground surface and plan view) along the Costa del Canneto slope showing the location of the single-station ambient noise measurements; (b–h) the HVNSR elaborated curves corresponding to the single-station measurement locations along the slope.

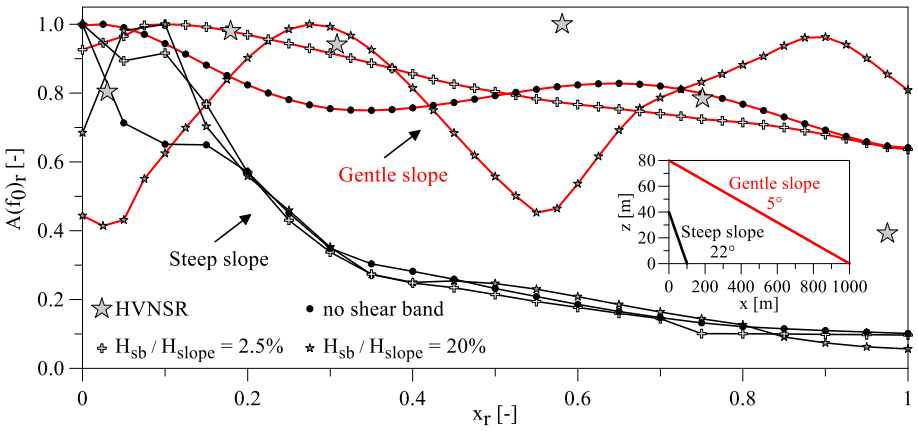

Fig. 7. Variation along the slope of the normalised amplification $A(f_0, x_r)_r$ as retrieved from HVNSR measurements along Costa del Canneto slope, compared to those retrieved from numerical simulation for the ideal cases presented in Ref. [46], considering thickness ratios H_{sb}/H_{slope} equal to 0 % (no shear band), 2.5 % and 20 %.

peaks at different locations depending on the thickness of the shear band. It should be mentioned that the results of ideal slopes were analysed in terms of normalized amplification $A(f_0, x_r)_r$ profile also for points behind the crest and in front of the toe of the slope.

The comparison between the ideal case results and the ambient noise data for the investigated site is herein shown only for relative distance between 0 and 1 (Fig. 7), since the in-situ measurements were carried out only along the slope and not behind the crest and in front of the slope toe. It indicates that the HVNSR data align more closely with the numerical results expected for gentle slopes, as the Costa del Canneto area

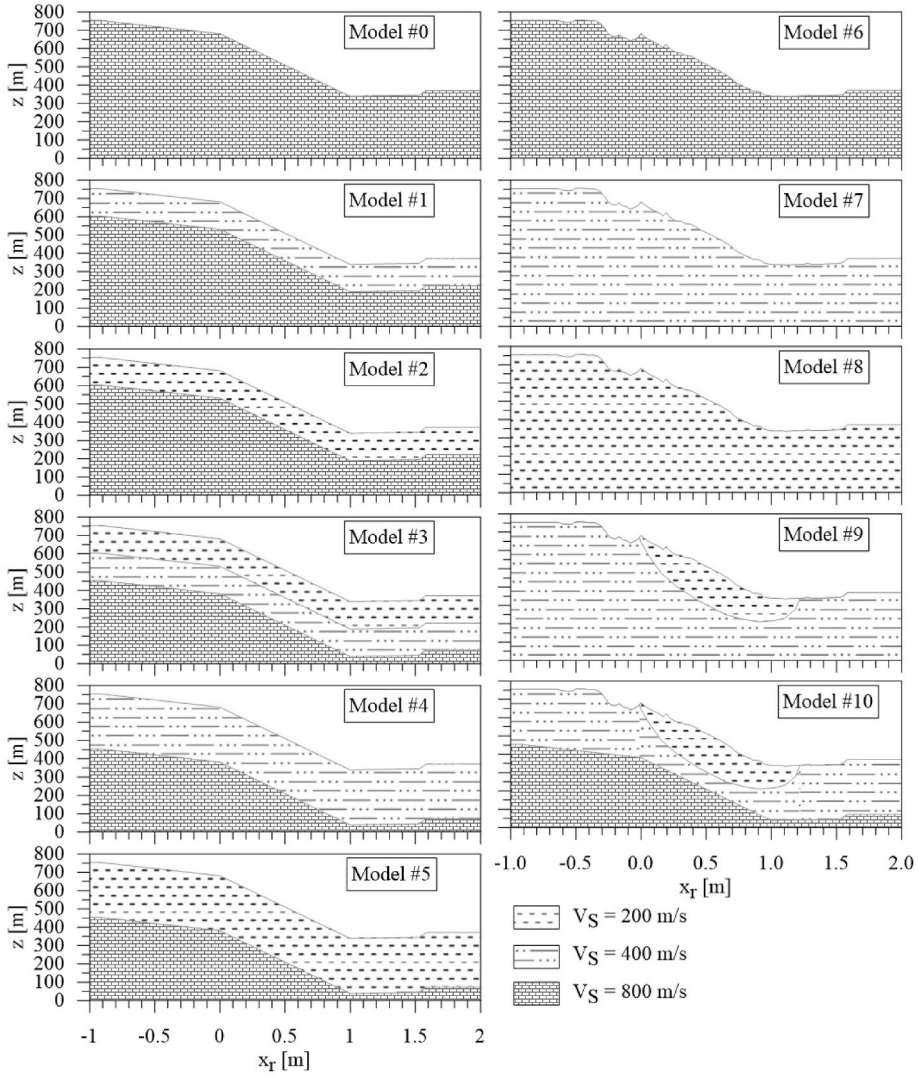

Fig. 8. Geotechnical slope models implemented in the numerical simulations for the parametrization stage considering layers with V_S constant with depth.

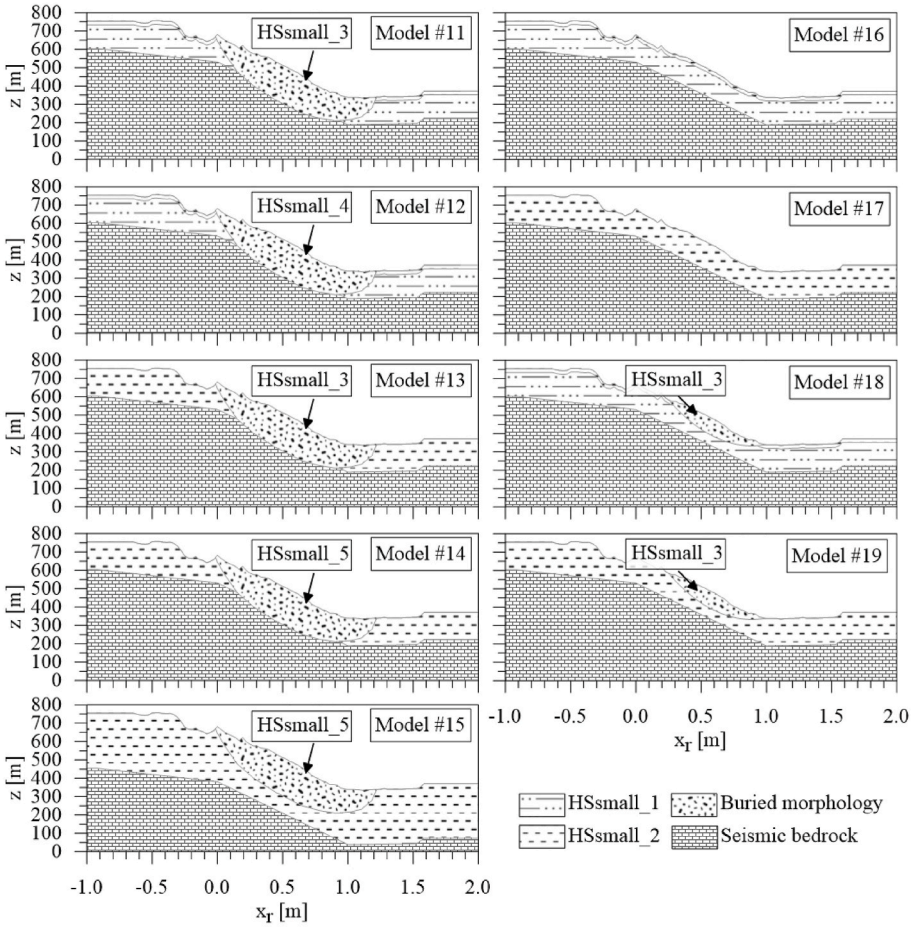

Fig. 9. Geotechnical slope models implemented in the numerical simulations for the parametrization stage considering layers with V_S increasing with depth.

Table 1
Summary of 2D numerical models considered in the subsoil parametrization (Models #0 to #10) assuming V_S constant with depth for each soil layer.

Model name	Topography	Subsoil stratigraphy	Constitutive model	Soil type/thickness
Model #0	Simplified	Homogeneous half-space	LVE	Seismic bedrock/-
Model #1	Simplified	Single-layered subsoil on seismic bedrock	LVE	Stiff soil/150 m
Model #2	Simplified	Single-layered subsoil on seismic bedrock	LVE	Soft soil/150 m
Model #3	Simplified	Two-layered subsoil on seismic bedrock	LVE	Soft soil/150 m Stiff soil/150 m
Model #4	Simplified	Single-layered subsoil on seismic bedrock	LVE	Stiff soil/300 m
Model #5	Simplified	Single-layered subsoil on seismic bedrock	LVE	Soft soil/300 m
Model #6	Realistic	Homogeneous half-space	LVE	Seismic bedrock/-
Model #7	Realistic	Homogeneous half-space	LVE	Stiff soil/-
Model #8	Realistic	Homogeneous half-space	LVE	Soft soil/-
Model #9	Realistic	Buried morphology in stiff soil half-space	LVE	Soft soil/variable up to 300 m
Model #10	Realistic	Buried morphology in single-layered subsoil on seismic bedrock	LVE	Soft soil/variable up to 300 m Stiff soil/300 m

is characterised by a mean slope of approximately 11°. Moreover, the values of $A(f_0, x_r)_r$ derived from the HVNSR measurements better comply with the numerical results obtained through slope models including a buried morphology (*i.e.*, H_{sb}/H_{slope} = 2.5% and 20% in Fig. 7), suggesting to consider, among others, numerical models which incorporate buried morphologies in the subsoil model parametrization stage (Step 3 of the methodology in Fig. 1).

3.4. Parametrization of the numerical subsoil models

The parametrization of the numerical subsoil models has been carried out based on the observations derived from the first two stages of the methodology and the comparison shown in Fig. 7. A total number of 20 subsoil models (named hereafter Model #0 to Model #19 in Figs. 8 and 9) have been specifically developed for the Costa del Canneto area, characterised by different complexities in terms of topography and subsoil settings. Since the parametrization procedure is iterative, the subsoil models have been constructed step by step, in order to obtain a good comparison between numerical and HVNSR results, on one hand, and to include the realistic subsoil setting, mostly representative of the recognised subsoil condition, on the other hand. The slope models are illustrated in Figs. 8 and 9, where L_{slope} has been identified considering the area along which the HVNSR measurements were performed, H_{slope} represents the height of the selected slope section, corresponding to the

Table 2
Summary of 2D numerical models considered in the subsoil parametrization (Models #11 to #19) assuming different V_S-depth law for each soil layer.

Model name	Topography	Subsoil stratigraphy	Constitutive model	Soil type/thickness
Model #11	Realistic	Buried morphology in two-layered subsoil on seismic bedrock	HSsmall	HSsmall_3/variable up to 200 m HSsmall_2/20 m HSsmall_1/130 m
Model #12	Realistic	Buried morphology in two-layered subsoil on seismic bedrock	HSsmall	HSsmall_4/variable up to 200 m HSsmall_2/20 m HSsmall_1/130 m
Model #13	Realistic	Buried morphology in single-layered subsoil on seismic bedrock	HSsmall	HSsmall_3/variable up to 200 m HSsmall_2/150 m
Model #14	Realistic	Buried morphology in single-layered subsoil on seismic bedrock	HSsmall	HSsmall_5/variable up to 200 m HSsmall_2/150 m
Model #15	Realistic	Buried morphology in single-layered subsoil on seismic bedrock	HSsmall	HSsmall_5/variable up to 200 m HSsmall_2/300 m
Model #16	Realistic	Two-layered subsoil on seismic bedrock	HSsmall	HSsmall_2/20 m HSsmall_1/130 m
Model #17	Realistic	Single-layered subsoil on seismic bedrock	HSsmall	HSsmall_2/150 m
Model #18	Realistic	Buried morphology in two-layered subsoil on seismic bedrock	HSsmall	HSsmall_3/variable up to 100 m HSsmall_2/20 m HSsmall_1/130 m
Model #19	Realistic	Buried morphology in single-layered subsoil on seismic bedrock	HSsmall	HSsmall_3/variable up to 100 m HSsmall_2/150 m

difference between the crest and the toe elevations, and $x_{0,slope}$ is the abscissa of the identified slope crest (Fig. 6a).

Three sets of 2D numerical models have been developed, as summarised in Table 1 and 2. The first set of numerical models (Table 1) considers a simplified topography, having the average inclination of the slope along section BB' (Figs. 3 and 6a), and simplified stratigraphic condition, including homogenous half-space, single-layered and two-layered stratifications (Models #0 to #5 in Fig. 8 and Table 1). Three types of soils have been considered, assuming a linear visco-elastic (LVE) constitutive model: a soft soil characterised by a shear wave velocity V_S equal to 200 m/s, a stiffer soil with V_S equal to 400 m/s and a bedrock material of V_S = 800 m/s. In detail, Model #0 is representative of a homogeneous bedrock half-space, defined to account for topographic conditions only; Model #1 and Model #2 are characterised by a single 150 m thick layer overlying the seismic bedrock; Model #3 is a two-layered slope characterised by a soft soil outcropping layer down to 150 m below ground surface (b.g.s.) overlying a 150 m thick layer of stiff soil, resting on the seismic bedrock; Model #4 and Model #5 are characterised by a single soil layer of 300 m thickness overlaying the seismic bedrock. In all these models, the stratigraphic contacts have been assumed parallel to the ground surface.

The second set of numerical models (Table 1) implements a more realistic topography, derived from the regional 5 × 5 m Digital Terrain Model (DTM) along the longitudinal section BB' (Figs. 3 and 6a), and possible buried morphologies, assuming the V_S of the soil layers constant with depth (Models #6 to #10 in Fig. 8 and Table 1). Specifically, Model #6, Model #7 and Model #8 consider a homogeneous visco-elastic half-space representing a seismic bedrock, a stiff soil and a soft soil deposit, respectively; Model #9 involves a buried morphology consisting of soft soils within a homogeneous stiff soil half-space; Model #10 is characterised by a homogeneous stiff soil layer extended down to 300 m b.g.s., overlying the seismic bedrock and including a buried morphology consisting of soft soil. It should be remarked that the buried morphology has been defined according to the geometry of the sliding surface recognised by Melidoro et al. [48], which has a maximum depth of about 200 m.

A third series of numerical models (Models #11 to #19 in Fig. 9 and Table 2) considers more realistic site conditions, implementing the real topography of the slope, the possible buried morphologies and the variation with depth of the shear wave velocity. To account for the increasing variation with depth of V_S, the Hardening Soil Model with small strain stiffness, HSsmall [61,62], has been adopted in the FE simulations. The constitutive model is capable to predict the nonlinear cyclic soil response and to account for the dependency with depth of the initial shear stiffness through Eq. (4):

$$G_0(z) = G_0^{ref} \cdot \left(\frac{c' \cos\varphi' - \sigma'_3 \sin\varphi'}{c' \cos\varphi' + p^{ref} \sin\varphi'} \right)^m \quad (4)$$

The calibration of the HSsmall model has been carried out with reference to the $V_S(z)$ profiles depicted in Fig. 4. A specific set of model parameters is associated to each soil type. In particular, HSsmall_1 parameters describe the behaviour of Soil_1 (Fig. 10a), HSsmall_2 parameters capture the $V_S(z)$ profile associated to Soil_2 (Fig. 10b), while HSsmall_3 parameters fit the $V_S(z)$ profile of Soil_3 (Fig. 10c). Based on the laboratory data available in the literature [48,54], the total unit weight γ, the effective friction angle φ' and the effective cohesion c' of the blue-grey clay have been assumed equal to 20 kN/m^3, 26° and 22 kPa, respectively. As for the yellow clay (Soil_2) and the reconstituted soil (Soil_3), strength parameters representative of a weaker material have been reasonably assumed. It should be mentioned that the selected c' and φ' values do not affect the numerical results of the seismic site response analyses, since a weak motion has been applied at the bottom of each FE slope model. Due to the absence of information about the hydraulic conditions within the area, no water table has been implemented in the numerical models, for the sake of simplicity. Thus, the $V_S(z)$ profiles for each soil type depend on the stress state in absence of water. For each soil type, the reference initial shear stiffness modulus G_0^{ref} and the parameter m are obtained by best fitting the $V_S(z)$ profile; the stiffness parameters E_{50}^{ref} and E_{oed}^{ref} are assumed to be equal to $E_{ur}^{ref}/3$, while the elastic unloading-reloading stiffness modulus E_{ur}^{ref} is equal to $G_{ur}^{ref}(1 + 2\nu')$ [10,69,70]. It is worth noting that a nonlinear response is not expected to be exhibited by the soils during the FE simulations, since a weak motion has been used as input in the dynamic analyses. Therefore, the model parameters pertaining to the soil cyclic response, *i.e.*, $\gamma_{0.7}$ and the ratio G_0^{ref}/G_{ur}^{ref}, are set equal to 0.04% and 5, respectively.

Additional $V_S(z)$ profiles have been considered in the simulations for Soil_3 (Fig. 10c), named HSsmall_4 and HSsmall_5. Specifically, HSsmall_4 represents a material characterised by a constant value of the shear wave velocity equal to 200 m/s, while HSsmall_5 describes a softer soil with increasing $V_S(z)$ profile and an average value of the shear wave velocity equal to 200 m/s. Table 3 summarises the list of the main HSsmall model parameters required to predict the $V_S(z)$ profiles of interest.

Model #11 presents a buried morphology characterised by the Hsmall_3 material within a stratification consisting of a HSsmall_2 layer extended down to 20 m b.g.s., overlying a 150 m thick HSsmall_1 layer, in turn underlain by the seismic bedrock. Model #12 presents the same stratigraphic condition of Model #11, except for the stiffness characteristics of the soil filling the buried morphology described by the

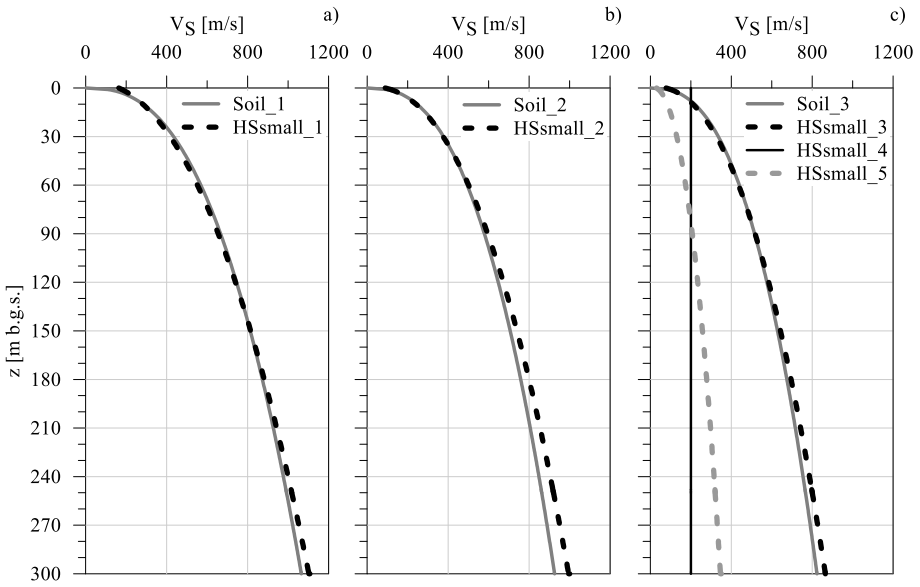

Fig. 10. $V_S(z)$ profiles predicted by HSsmall for a) Soil_1, b) Soil_2 and c) Soil_3.

Table 3
List of the adopted HSsmall parameters.

Parameter	Description	HSsmall_1	HSsmall_2	HSsmall_3	HSsmall_4	HSsmall_5
E_{50}^{ref} [kPa]	Reference secant stiffness in standard drained triaxial test	23,780	15,530	11,743	11,743	1957
E_{oed}^{ref} [kPa]	Reference tangent stiffness for primary oedometer loading test	23,780	15,530	11,743	11,743	1957
E_{ur}^{ref} [kPa]	Reference unloading/reloading stiffness at engineering strains	71,339	46,591	35,229	35,229	5872
ν_{ur} [−]	Poisson's ratio for unloading/reloading	0.2	0.2	0.2	0.2	0.2
G_0^{ref} [kPa]	Reference shear modulus at very small strains	148,624	97,064	73,394	73,394	11,743
m	Power for the stress-level dependency of stiffness	0.89	0.86	0.86	0.00	0.86
γ [kN/m^3]	Unit weight	20	19	18	18	18
c' [kPa]	Effective cohesion	22	5	5	5	5
φ' [°]	Effective friction angle	26	22	22	22	22
p'_{ref} [kPa]	Reference stress for stiffness	100	100	100	100	100

HSsmall_4 parameters. Model #13 is characterised by a buried morphology characterised by the Hsmall_3 within a HSsmall_2 layer extending down to 150 m b.g.s. overlying the seismic bedrock. Model #14 includes a buried morphology characterised by the soft material named HSsmall_5 within a layer of 150 m thick HSsmall_2 material overlying the seismic bedrock. In all these models, for most of the slope the softer material characterising the buried morphology is in direct contact with the seismic bedrock. The interface between the soft material and the bedrock is placed at a maximum depth of approximately 200 m. Model #15 presents a HSsmall_2 layer extended down to 300 m b.g.s. overlying the seismic bedrock and a buried morphology characterised by the softer material HSsmall_5.

To highlight the effect of solely the vertical stratigraphic heterogeneity, Model #16 and Model #17 have been included in the parametrization, while Models #18 and #19 have been implemented to highlight the effect of a shallower buried morphology. In detail, Model #16 is characterised by a 20 m thick soft soil layer (*i.e.*, HSsmall_2) overlying a stiffer material (*i.e.*, HSsmall_1), extended down to the seismic bedrock located 150 m b.g.s.; Model #17 is composed by a soft HSsmall_2 layer extended down to the seismic bedrock located 150 m b.g.s.; Model #18 considers a shallower HSsmall_3 buried morphology with a maximum depth of 100 m resting within a two-layered subsoil composed by a 20 m thick layer of the soft HSsmall_2 material overlying the stiffer HSsmall_1 extending down to the seismic bedrock located 150 m b.g.s. Finally, Model #19 is characterised by the soft HSsmall_2 layer down to the seismic bedrock located 150 m b.g.s. and a shallow HSsmall_3 buried morphology with a maximum depth of 100 m.

All the numerical simulations have been carried out adopting as reference signal a simple Ricker pulse (Eq. (5)) with a maximum acceleration of 0.01g (Fig. 11a):

$$a(t) = \left(1 - 2\pi^2 f_c^2 t^2\right)\exp\left(-\pi^2 f_c^2 t^2\right) \quad (5)$$

A central frequency, f_c, of 0.4 Hz has been chosen to produce a broadband energy in the bandwidth of frequencies 0.2–0.6 Hz (Fig. 11b), which is consistent with the fundamental frequencies of the subsoil in the area of interest (*i.e.*, 0.19–0.25 Hz).

The dissipative capacity of the soils considered in all the numerical models has been implemented through the viscous Rayleigh damping formulation [71,72], considering a target damping of 0.1% and two control frequencies equal to 0.1 Hz and 1.0 Hz (Fig. 11b) [73,74].

The dynamic boundary conditions have been implemented as free-field boundaries along the vertical sides of the finite element models, complemented by fixed vertical displacements, while a compliant base (*i.e.*, adsorbing boundary) at the bottom of the mesh has been imposed to emulate the wave dissipation into the deeper soil layers with minimal reflection at the lower boundary [75,76]. The compliant base option involves the application of the upward propagating component of the reference signal at the FE model base only. Thus, the input signal undergoes a conversion by the FE code into a shear stress time history. Consequently, the accelerogram at the base of the numerical models emerges as an output of the numerical simulation and it is not pre-determined. Additionally, the lateral extension of the FE meshes has been set equal to five times the height of the model, to mitigate any potential interference of the vertical boundaries with the slope area [77]. To guarantee numerical accuracy, the coarseness of the FE mesh has been adjusted, ensuring a distance between two consecutive nodes

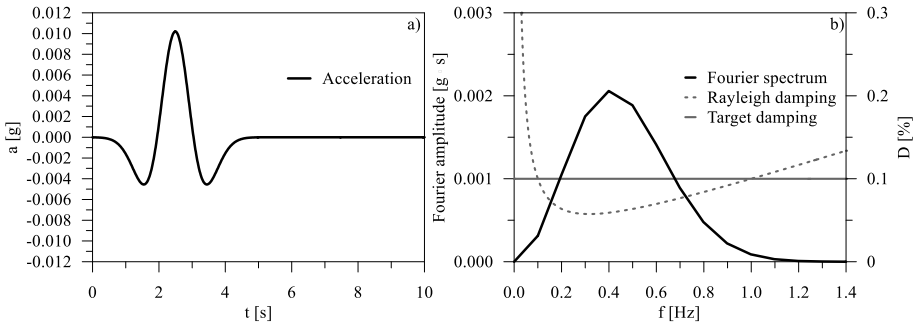

Fig. 11. Ricker reference signal: a) acceleration time history and b) Fourier response spectrum. The variation of Rayleigh damping with frequency is also shown in the same figure.

smaller than approximately one-eighth of the wavelength associated with the maximum frequency content, denoted as f_{max}, of the input wave [78]. For this case study, f_{max} has been selected as 1 Hz. The gravity loading procedure has been implemented to establish the initial stress state before subjecting the FE slope models to the dynamic phase.

3.5. Comparison of HVNSR data and numerical results

The results of the dynamic simulations of the different geotechnical subsoil models are presented here in terms of normalised amplification $A(f_0, x_r)_r$ profiles (Eq. (1)) and compared with the HVNSR in-situ measurements.

When homogeneous half-space numerical models are considered, $A(f_0, x_r)_r$ has been evaluated as the ratio between the Fourier spectrum of the acceleration recorded at ground surface and the Fourier spectrum of the reference signal. Instead, when a vertical heterogeneity or a buried morphology is implemented in the numerical model, $A(f_0, x_r)_r$ has been evaluated as the ratio of the ground surface Fourier spectrum and the Fourier spectrum of the signal recorded at the same abscissa but at the interface between the soil deposit and the seismic bedrock.

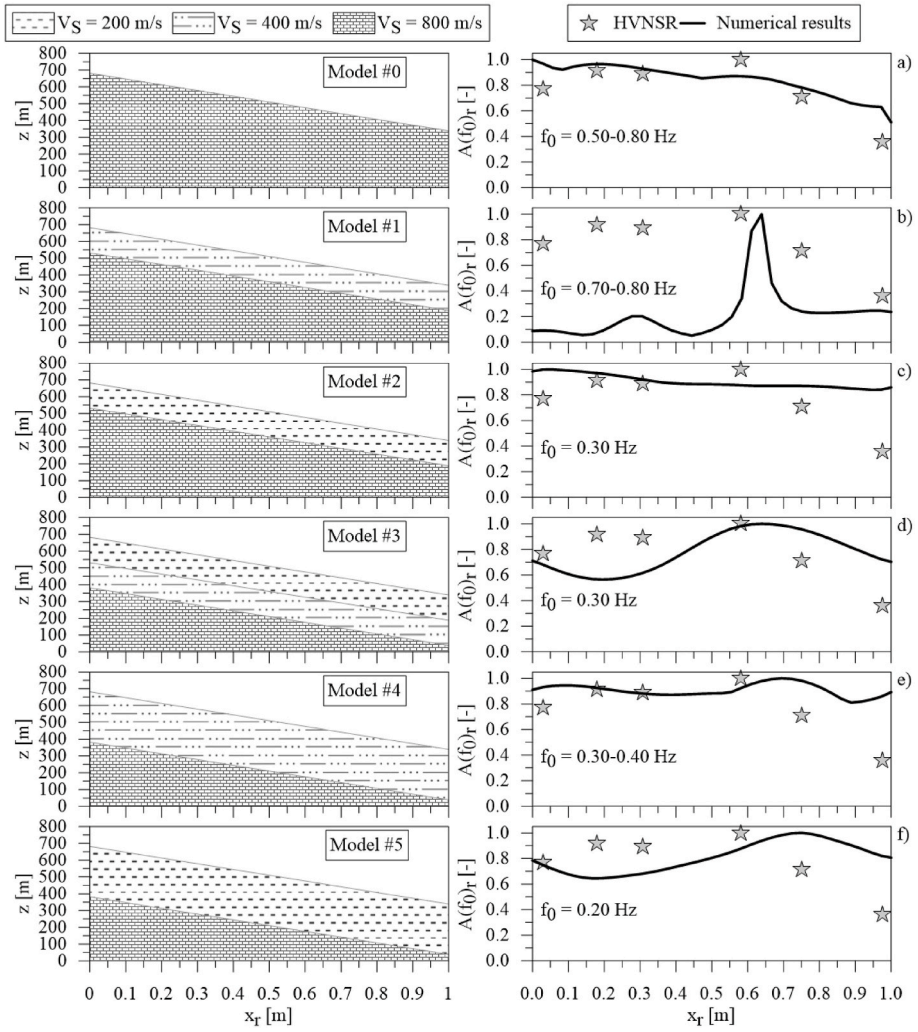

Fig. 12. Left side: geotechnical models considering simplified topography and buried morphologies and assuming V_S constant with depth. Right side: comparison of HVNSR and numerical results.

The results of the first set of numerical simulations (Fig. 8 and Table 1), characterised by a simplified topographic and stratigraphic conditions, are shown in Fig. 12, together with the HVNSR data at different observation points along the slope. Fig. 12a reports the $A(f_0, x_r)_r$ obtained for the rigid homogeneous half-space, *i.e.* Model #0, representative of those cases where only topographic amplifications can occur, showing a decreasing pattern along the slope. The interaction between topographic and stratigraphic effects, accounted for by the geotechnical Models #1 to #5, strongly influences the distribution of the normalised amplification along the slope (Fig. 12b–f), presenting different patterns characterised by peaks of different amplitudes at different location along the slope. In the figures, the ranges of the fundamental frequency f_0 predicted by each numerical model along the slope are also reported. The direct comparison of the numerical predictions with the HVNSR measurements suggests that none of the proposed geotechnical models is suitable for representing the subsoil conditions in the examined area, except for Model #0.

The adoption of the real topography of the area in the numerical models allows to slightly improve the distribution of the normalised amplification $A(f_0)_r$ along the slope, as shown in Fig. 13. Indeed, for the case of the outcropping seismic bedrock ($V_S = 800$ m/s), the Model #6 profile (Fig. 13a) seems to be more consistent with the HVNSR results than Model #0 (Fig. 12a), suggesting that the topography is capable to bias the site response at the ground surface. Moreover, the stiffness properties of the homogeneous half-space also influence the amplification at the ground surface, as shown in Figs. 13b and c illustrating the results of Model #7 and Model #8, respectively. In particular, if the shear wave velocity is equal to 200 m/s (Model #8), the motion tends to be amplified in the upper portion of the slope more than around the toe (Fig. 13c); conversely, the $A(f_0)_r$ profile is equally distributed along the slope surface, with values between 0.8 and 1, when the homogeneous half-space is characterised by a stiffer soil, *i.e.* $V_S = 400$ m/s (Fig. 13b). The comparison of such results with the field data is fairly good for the Model #7 case, despite the numerical prediction underestimates the $A(f_0)_r$ for $x_r = 0.6$ and overestimates the $A(f_0)_r$ for x_r equal to about 1.0 (Fig. 13b). The Model #8, instead, provides a general underestimation of $A(f_0)_r$, which increases around the toe of the slope (Fig. 13c). However, these configurations of the subsoil setting should be excluded since a stratified condition has been already recognised in the prototype area. Indeed, softer clays are observed to outcrop at ground surface and the underlying stiffer clay is expected to extend down to 400–500 m.

When a buried morphology is introduced in the numerical models, *i.e.* Model #9 and Model #10, the normalised amplification $A(f_0)_r$ profiles achieve maximum values at relative distances around 0.4 and 0.6 for Model #9 and Model #10, respectively, and reduce to values between 0.2 and 0.4 after the peaks (Fig. 13d and e).

For all the analysed models, the numerical predictions are not in satisfactory agreement with the HVNSR data, suggesting the need for an improvement of the subsoil model by implementing the variation with depth of the shear stiffness and different soil stratification and geometries of the buried morphology, as done with the Models #11 – #19. The results of Models #11 to #15, with deep buried morphologies, are shown in Fig. 14, while Fig. 15 reports the output obtained from Models #16 to #19 characterised by shallower buried morphologies.

The presence of a deep buried morphology of different stiffness (Models #11 to #15) strongly differentiates the slope seismic response, providing $A(f_0)_r$ along the slope characterised by peaks at relative distance x_r in the range 0.15–0.60. Specifically, the change of soil stiffness within the buried morphology (Model #11 *vs* Model #12) produces similar results in terms of amplitude of the $A(f_0)_r$ profile along the slope,

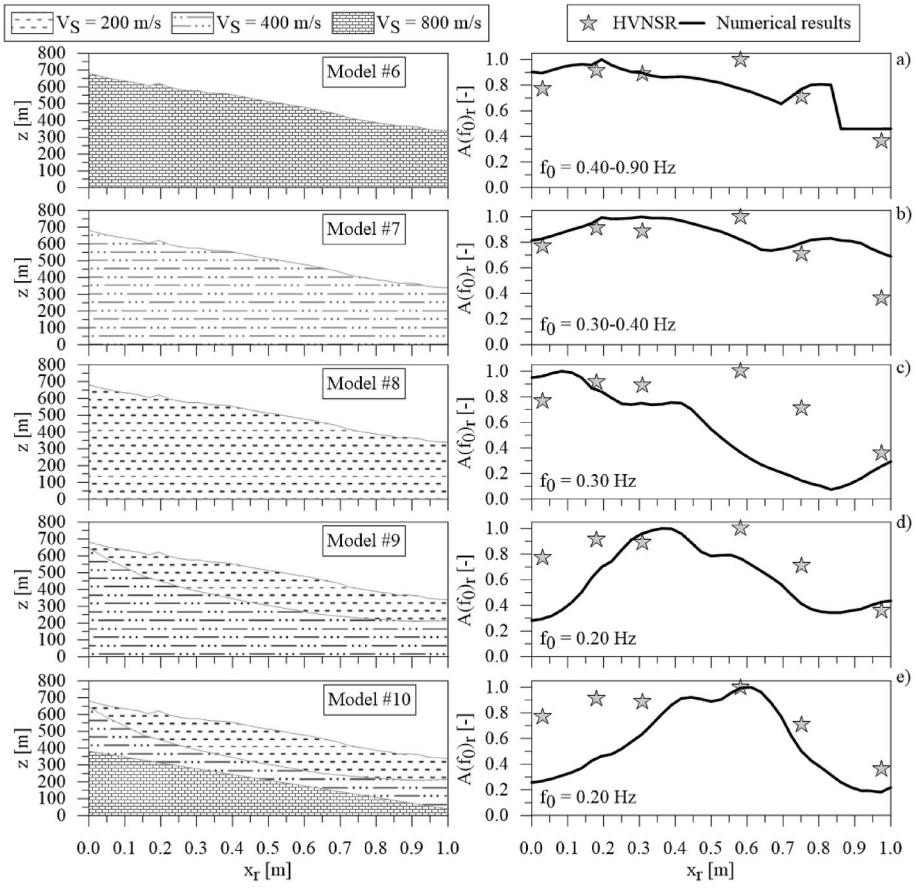

Fig. 13. Left side: geotechnical slope models considering reliable geometries for both the topography and the buried morphology and assuming V_S constant with depth. Right side: comparison of HVNSR and numerical results.

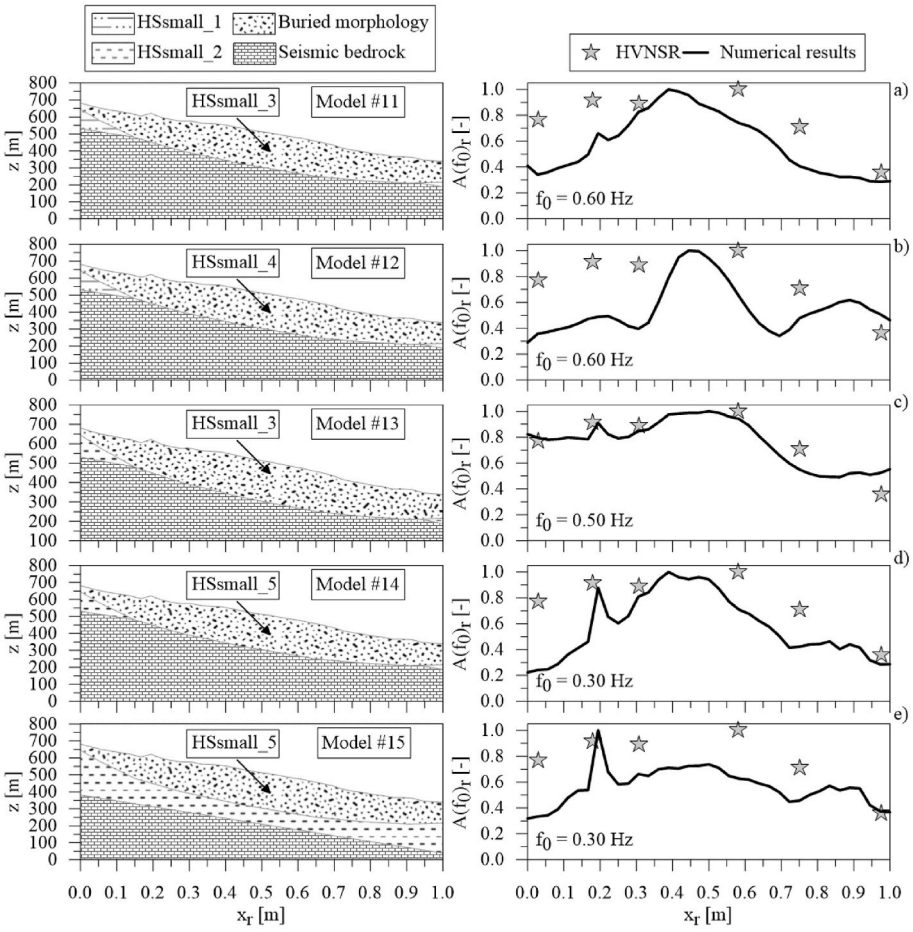

Fig. 14. Left side: geotechnical slope models considering a reliable topography, a deep buried morphology and assuming V_S increasing with depth. Right side: comparison of HVNSR and numerical results.

despite its shape is slightly different. However, the peaks are located at about the same relative distance of 0.4. The $A(f_0)_r$ profile tend to show an additional peak at $x_r = 0.2$ if the 150–300 m thick outcropping layer within the slope is formed of HSsmall_2, whatever the buried morphology is (Models #13, #14 and #15). The Model #14, characterised by lower stiffness of the soil within the buried morphology, tend to amplify the seismic motion at the top of the slope less than the Model #13, this latter showing a regular distribution with high values of the normalised amplification. Then, a deeper location of the seismic bedrock provides a smaller amplification of the motion in the middle portion of the slope and a higher amplification at the top and around its toe with respect to the case of shallower seismic bedrock (Model #14 *vs* Model #15).

The vertical stratigraphic heterogeneity of the slope deposits differently amplifies the input motion at the ground surface (Model #16 *vs* Model #17 in Fig. 15). Indeed, the $A(f_0, x_r)_r$ for Model #16 presents high values of about 0.8-1 around the top of the slope and significantly reduces along the slope, achieving values of 0.3–0.4 around its toe (Fig. 15a). Conversely, the Model #17 results show a regular distribution of the amplification, characterised by high values between 0.8 and 1, which tend to slightly decrease to 0.6 at the toe of the slope (Fig. 15b).

Finally, a shallower buried morphology filled with HSsmall_3 material (implemented in the Models #18 and #19) further modifies the response at the ground surface. In particular, the comparison between Model #16 and Model #18 suggests that the buried morphology tend to amplify the motion also in the middle portion of the slope where it is located (*i.e.*, $x_r = 0.25$–0.95). Moreover, the comparison of the numerical results predicted by the Models #14 and #19 indicates that the deeper buried morphology (Model #14) tends to amplify the motion in the middle portion of the slope more than the shallower one (Model #19).

4. Discussion

The goodness of the numerical procedure to predict the in-situ measurements has been evaluated through the one-to-one comparison between the normalised amplification $A(f_0, x_r)_r$ calculated for the slope models (*i.e.* $A(f_0)_{r\_FEM}$) and those estimated from the HVNSR data (*i.e.* $A(f_0)_{r\_HVNSR}$) at each location of measurement. Fig. 16a shows the scatter plots between $A(f_0)_{r\_HVNSR}$ obtained from HVNSR data and $A(f_0)_{r\_FEM}$ derived from the numerical simulations for all the slope models. Among the others, Models #0, #2, #4, #6, #7, #13, #17, #18, and #19 provide a fairly good fitting with the in-situ data, since at least three of the six points (representing the response at different location along the slope) fall within the limits of ±15%, as provided by Eq. (6). These observations are also confirmed by the median values of the absolute error distribution (Fig. 16c), quantified for each slope model at different locations with Eq. (7).

$$\begin{aligned} X \le A(f_0)_{r\_FEM} \le Y \\ X = A(f_0)_{r\_HVNSR} - 0.15 \cdot A(f_0)_{r\_HVNSR} \\ Y = A(f_0)_{r\_HVNSR} + 0.15 \cdot A(f_0)_{r\_HVNSR} \end{aligned} \quad (6)$$

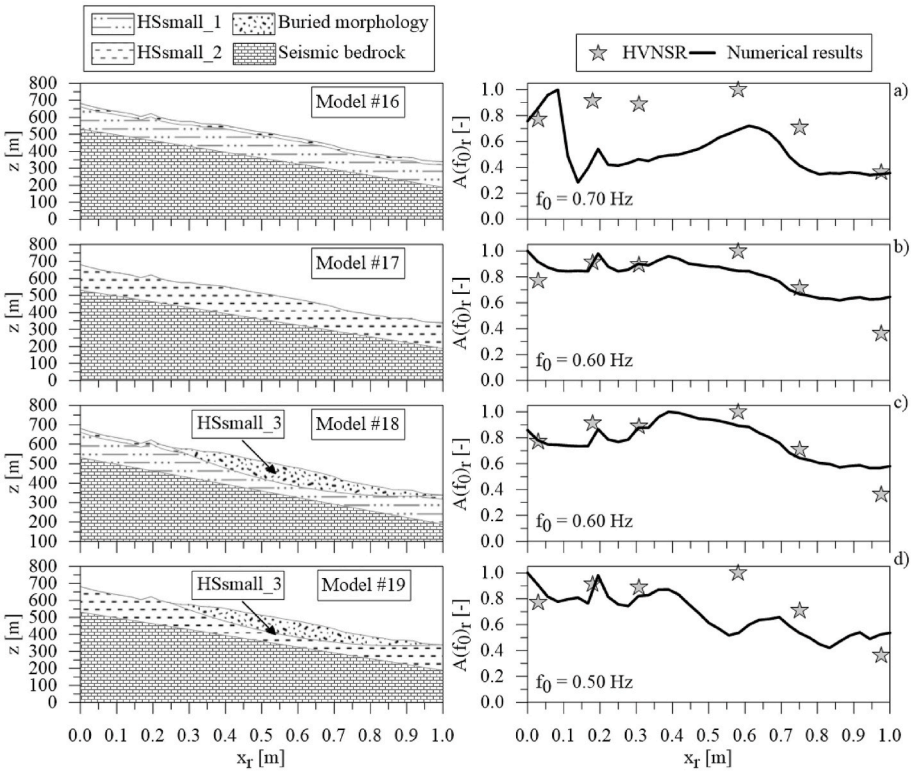

Fig. 15. Left side: geotechnical slope models considering a reliable topography, a shallow buried morphology and assuming V_S increasing with depth. Right side: comparison of HVNSR and numerical results.

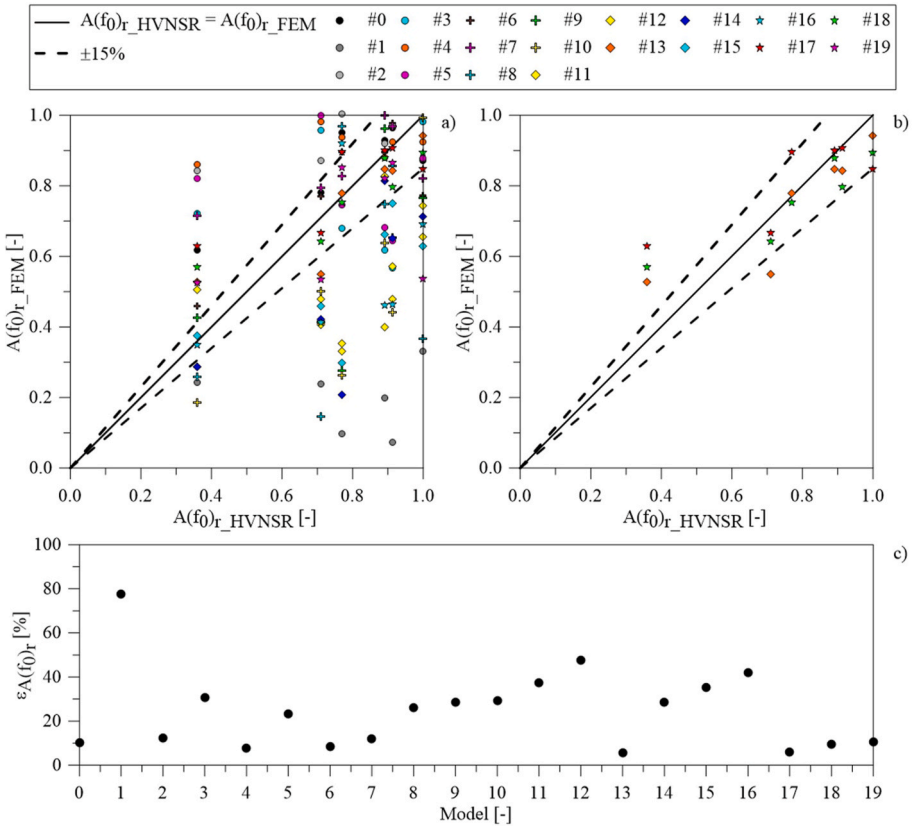

Fig. 16. Scatter plots between $A(f_0)_{r\_HVNSR}$ from HVNSR data and $A(f_0)_{r\_FEM}$ from numerical simulations (a) for all the slope models and (b) for the Models #13, #17 and #18; (c) median values of the error distribution obtained for all the slope models.

$$\varepsilon_{A(f_0)_r} = \left| \frac{A(f_0)_{r\_HVNSR} - A(f_0)_{r\_FEM}}{A(f_0)_{r\_HVNSR}} \right| \quad (7)$$

The plot in Fig. 16c indicates that the median value of the absolute error is higher than 15 % for most of the slope models (*i.e.*, Models #1, #3, #5, #8, #9, #10, #11, #12, #14, #15, #16), suggesting to exclude them because of the poor fitting of the numerical results with the HVNSR data. Conversely, Models #0, #2, #4, #6, #7, #13, #17, #18 and #19 exhibit median values of $\varepsilon_{A(f_0)_r}$ below 15%, advising to further investigate the possibility of considering those models as representative of the subsoil condition of the examined area. Among these, Model #0 should be excluded, as it implements a simplified topography and an outcropping seismic bedrock, which is far from the real site condition; Models #2 and #4 implement a simplified topography and a constant shear wave velocity profile, again poorly representative of the site conditions; Models #6 and #7 could be disregarded, as they assume a homogeneous subsoil condition, which is inconsistent with the site evidences which recognise a stratified soil deposit; Model #19 should be neglected since it fails to capture the increase of the normalised amplification $A(f_0)_r$ in the middle of the slope (Fig. 15d).

Among all the dynamic simulations, the most satisfactory agreement between the numerical predictions and the HVNSR data is provided by the Models #13 (Fig. 14c), #17 (Fig. 15b) and #18 (Fig. 15c), for which the normalised amplification $A(f_0)_r$ profiles retrieved from numerical simulations show a trend similar to the one identified by the HVNSR data, as summarised in Fig. 17a. Indeed, Model #17 shows results more similar to HVNSR than the other models at $x_r = 0.2$, and both Models #17 and #18 demonstrate a good agreement with the HVNSR results at $x_r = 0.75$. Model #13 seems, instead, to capture the HVNSR data over the entire range of x_r. To highlight the differences between the three best-fitting slope models in terms of their dynamic characteristics, the $V_S(z)$ profiles retrieved at the relative distances of 0.11, 0.50 and 0.92, *i.e.* in the upslope, mid-slope and downslope portion of the model, are sketched in Fig. 17b, c and d, respectively. These specific verticals have been selected for their location in parts of the slope characterised by a great variability in terms of stratigraphic conditions, which leads to different ground amplifications. It might be observed that the $V_S(z)$ profiles of the three slope models are similar to each other, although characterised by different trends with depth.

To summarise, the investigation seems to suggest that the slope of interest is characterised by the presence of a buried morphology (Models #13 and #18) or, in general, by the location of a seismic bedrock at depths higher than 100 m (Model #17). Therefore, additional geotechnical site investigations (*e.g.*, continuous coring borehole, inclinometers, down-hole tests, etc.) reaching a depth of at least 100 m need to be conducted with the aim to better constrain the lateral and vertical variation of soil mechanical properties within the deposit and to investigate the shape of the possible buried morphology.

Finally, to investigate the role of the applied input motion on the reliability of the proposed methodology, additional dynamic simulations

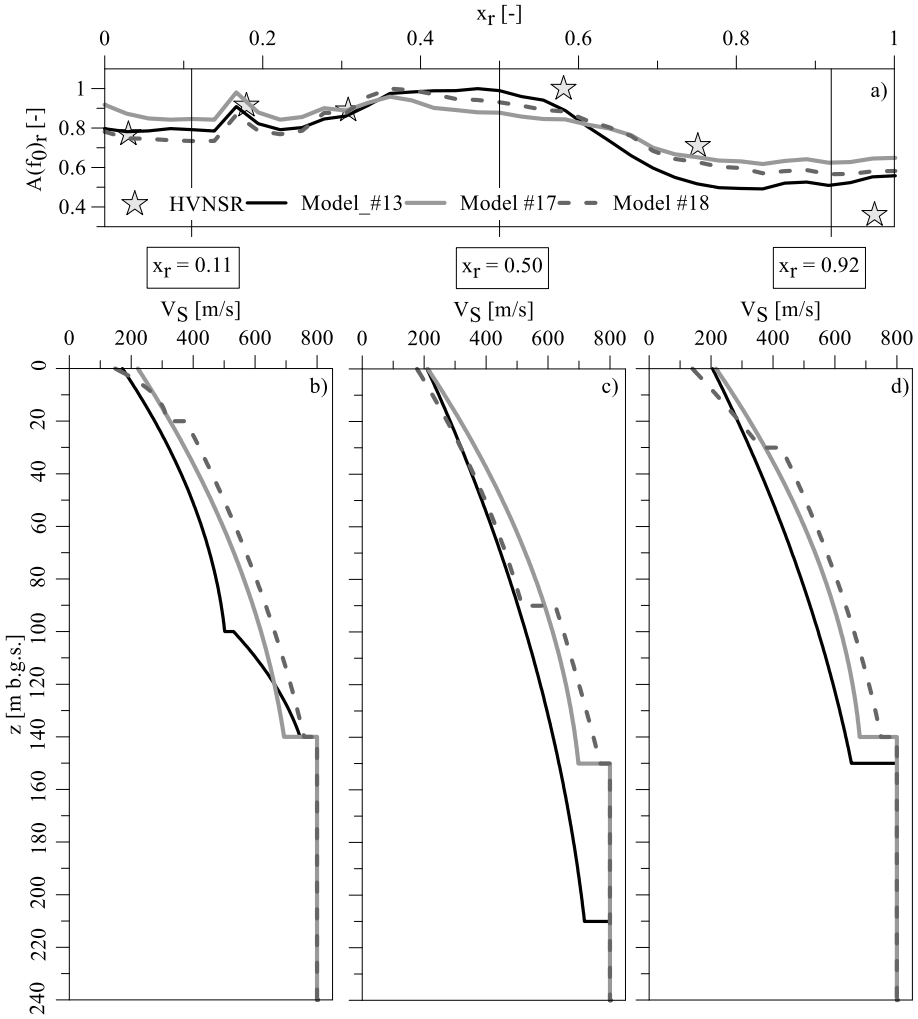

Fig. 17. a) comparison of HVNSR data and numerical results from the Models #13, #17 and #18; b-d) $V_S(z)$ profiles implemented in the Models #13, #17, and #18 along three different verticals.

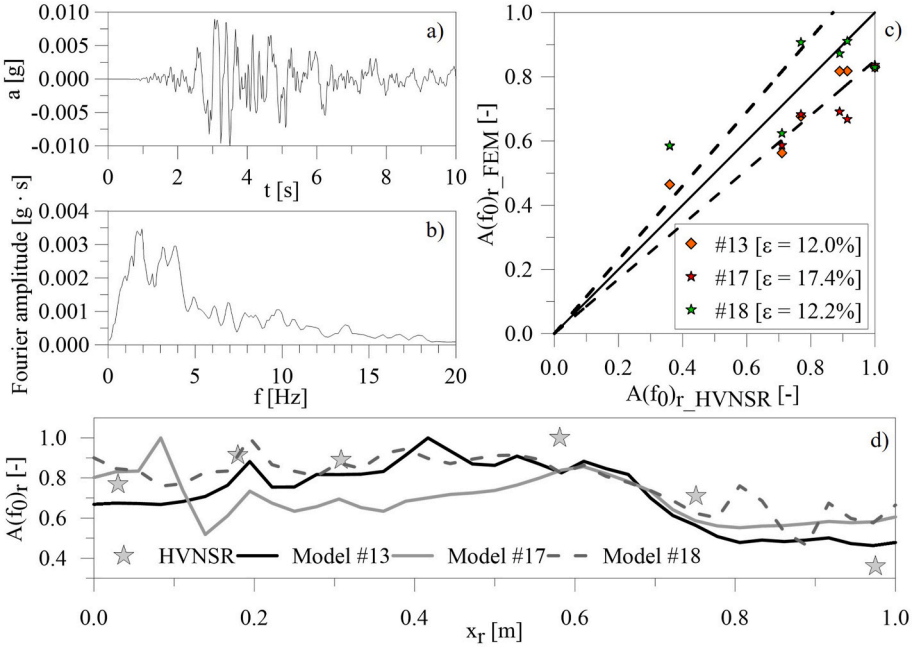

Fig. 18. (a) Acceleration time history, (b) Fourier spectrum of the earthquake recorded at the Cascia station (Italy) occurred on the July 14, 1997 and (c) scatter plot of $A(f_0)_{r\_HVNSR}$ compared to $A(f_0)_{r\_FEM}$ for the Models #13, #17 and #18; (d) comparison of HVNSR data and numerical results for the Models #13, #17 and #18.

have been conducted with reference to the best-fitting Models #13, #17 and #18 by applying a real earthquake scaled to a PGA of 0.01g as input motion (Fig. 18a and b). The acceleration time history recorded at the Cascia station (Italy) during the earthquake occurred on the July 14, 1997 has been adopted in this case. The results of the 2D numerical analyses have been elaborated in terms of normalised amplification $A(f_0, x_r)_r$ profile and compared with the HVNSR data (Fig. 18c and d). The resulting $A(f_0, x_r)_r$ profiles are characterised by trends similar to those predicted by the simulations performed using the wavelet signal, highlighting a fairly good agreement with the HVNSR data at least with reference to Model #13 and #18, both characterised by median values of the absolute error equal to about 12 % (Fig. 18c). This proves that the numerical results are not particularly sensitive to the applied input motion.

The most important advantage of the proposed methodology is that, starting from few geological, geomorphological and geotechnical data, retrieved from historical archives, and several focused ambient noise measurements, a plausible and reliable geotechnical subsoil model could be obtained also in areas characterised by the presence of buried morphologies. However, this should be further confirmed through additional in-depth, properly designed site investigations. The methodology provides a tool to interpret the data from expeditive in-situ measurement and to elaborate possible 2D subsoil settings. Nevertheless, as any engineering methodology, the proposed approach has some drawbacks and limitations. At first, the identification of a reliable subsoil model depends on the engineering judgement of the user, which should be able to collect all the available data (geological, geomorphological and geotechnical data) in order to develop a first attempt of the subsoil model, that should be then refined through a cut-and-try approach until the numerical results are comparable to the HVNSR data. Moreover, it requires a non-trivial computational effort. As a general indication about the expected computational time, approximately 2–3 working days are needed to conduct a 2D numerical simulation of one slope model, retrieve the outputs referenced to points spaced 20 m apart, and derive the $A(f_0)_r$ profile.

Secondly, it is suggested to apply the methodology described in this work only in cases where the site conditions allow to neglect the 3D effects usually occurring in the wave propagation process. Indeed, the HVNSR measurements are able to capture the 3D response of the subsoil deposit, while the numerical modelling is performed adopting a 2D geometrical scheme. This latter assumption could bias the predicted slope behaviour and affect the comparison between the numerical results and in-situ data. Indeed, the possible three-dimensionality in the seismic wave propagation through the slope, related not only to the topographic, but also to the subsoil conditions, could be considered the culprit of the disagreement between measured and predicted data. On the contrary, the 2D FE numerical modelling can be consistently employed to assess the slope seismic response in cases where the analysis of the HVNSR directionality indicates the absence of significant 3D effects. In the specific case of Costa del Canneto slope, the spectra of the two horizontal components of seismic ambient noise measurements (not shown herein for the sake of brevity) exhibit highly comparable trends, without revealing substantial differences across large portions of the spectrum. Despite some degree of three-dimensionality might always be recognised, the assumption of negligible 3D effects is deemed to be a reasonable first approximation in the presented case study, justifying the adoption of 2D FE numerical modelling.

5. Conclusions

The paper proposes a new methodological procedure for the identification of preliminary subsoil models, based on the joint integration of seismic ambient noise measurements and 2D numerical analyses of the site response of slopes, opportunely built to get the best agreement between the numerical results and in-situ data. The approach is thought to be applied for the characterisation of slope areas characterised by uneven topography and complex subsoil conditions, also presenting buried lithological bodies of uncertain morphology, for which very few geological and geotechnical data are available, most often coming from either previous geognostic campaigns or from the literature. In these cases, the execution of site surveys, laboratory and in-situ testing and monitoring, required for the subsoil characterisation, could be very expensive. It should be mentioned that the proposed methodology might also be applied to flat areas, where complex subsoil conditions might be detected. The proposed approach is intended to serve as a cost-effective and less invasive tool to reduce the uncertainties associated with the

geological, geomorphological and geotechnical characterisation of the area and to guide the design of in-depth site investigations. Moreover, the proposed methodology is not meant to be alternative to the existing procedures for the interpretation of the HVNSR curves, while it should be considered as a tool to identify a possible subsoil model through the joint interpretation of HVNSR data and 2D numerical results. The greatest strength of the proposed procedure is the possibility to include potential buried morphologies in the 2D numerical models of the sloping area, that otherwise could not be incorporated into 1D numerical schemes.

The methodological approach has been applied to the prototype slope of Costa del Canneto in the South of Italy, selected for the limited availability of direct geotechnical information. After retrieving and collecting the existing geological, geomorphological and geotechnical data for the area of interest from the literature, non-invasive geophysical surveys have been conducted with the aim to guide the process of parametrization of the subsoil setting. The elaboration of the ambient noise measurements suggested the presence of a complex vertical heterogeneity or a buried morphology in the soil deposit and provided useful information for the parametrization of the subsoil models. Based on the comparison between the HVNSR measurements and the results of 2D numerical seismic response analyses of various slope models using weak Ricker wavelet input motions, an iterative process of subsoil model parametrization has been conducted, accounting, at each step, for the results of the previous simulations. In the specific case study, the direct comparison of the in-situ data and the numerical results allowed to reduce the possible geotechnical subsoil models to a small number of realistic subsoil configurations, which then need to be validated through detailed geotechnical investigations. Indeed, the shear wave velocity distribution with depth and along the slope of the three most credible models identified for the Costa del Canneto case study are very similar to each other and no conclusive definition of the real subsoil setting of the investigated area can be derived from the analyses. Hence, further in-situ geotechnical investigations are strongly recommended to better characterise the stratigraphy of the area and constrain the geometry of the buried morphology, if recognised to be present.

CRediT authorship contribution statement

Gaetano Falcone: Writing – review & editing, Writing – original draft, Visualization, Validation, Methodology, Formal analysis, Data curation, Supervision, Conceptualization. **Annamaria di Lernia:** Writing – review & editing, Writing – original draft, Validation, Methodology, Conceptualization, Formal analysis, Supervision, Visualization. **Giuseppe Calamita:** Writing – review & editing, Writing – original draft, Investigation, Data curation, Supervision. **Maria Rosaria Gallipoli:** Writing – review & editing, Supervision, Data curation, Investigation, Writing – original draft. **Angela Perrone:** Writing – review & editing, Investigation, Data curation, Writing – original draft. **Sabatino Piscitelli:** Investigation, Data curation, Writing – review & editing. **Jessica Bellanova:** Investigation, Data curation, Writing – review & editing. **Francesco Cafaro:** Writing – review & editing, Supervision, Resources, Project administration, Funding acquisition. **Gaetano Elia:** Writing – review & editing, Supervision, Resources, Conceptualization, Funding acquisition, Project administration, Writing – original draft.

Declaration of competing interest

The authors declare that they have no known competing financial interests or personal relationships that could have appeared to influence the work reported in this paper.

Acknowledgments

The support received from the PON-MITIGO project (PON Programma R&I 2014–2020: MITIGO, ARS01_00964) is acknowledged. The last author is grateful for the financial support provided by the projects "National research Center for HPC, Big Data and Quantum Computing – Spoke 5: Environment and Natural Disasters" (CN_00000013) and "MOST – Sustainable Mobility National Research Center – Spoke 7" (CN_00000023), both funded by the European Union - Next Generation EU within the National Recovery and Resilience Plan (M4, C2, I1.4). The first author acknowledges the financial support received from the "GRINS - Growing Resilient, INclusive and Sustainable" project (GRINS PE00000018 - CUP E63C22002000002), funded by the European Union - Next Generation EU within the National Recovery and Resilience Plan (M4, C2, I1.3). The manuscript reflects only the authors' views and opinions. Neither the European Union nor the European Commission can be considered responsible for them. The authors sincerely thank prof. Alessandro Guerricchio for his valuable suggestions and Cotecchia Associates for providing the Ferrandina-Matera railway project documentation.

Data availability

Data will be made available on request.

References

[1] Ansal A, Tönük G, Kurtulus A. Microzonation for urban planning. Geotech Geol Earthq Eng 2009;11:133–52. https://doi.org/10.1007/978-90-481-2399-5_9.
[2] De Risi R, Penna A, Simonelli AL. Seismic risk at urban scale: the role of site response analysis. Soil Dynam Earthq Eng 2019;123:320–36.
[3] Mori F, Gena A, Mendicelli A, Naso G, Spina D. Seismic emergency system evaluation: the role of seismic hazard and local effects. Eng Geol 2020;270:105587. https://doi.org/10.1016/j.enggeo.2020.105587.
[4] Sabetta F, Fiorentino G, Bocchi F, Sinibaldi M, Falcone G, Mendicelli A. Influence of local site effects on seismic risk maps and ranking of Italian municipalities. Bull Earthq Eng 2023:1–28. https://doi.org/10.1007/S10518-023-01619-9/TABLES/12.
[5] van Ginkel J, Ruigrok E, Stafleu J, Herber R. Development of a seismic site-response zonation map for The Netherlands. Nat Hazards Earth Syst Sci 2022;22:41–63. https://doi.org/10.5194/NHESS-22-41-2022.
[6] Del Gaudio V, Pierri P, Calcagnile G. Analysis of seismic hazard in landslide-prone regions: criteria and example for an area of Daunia (southern Italy). Nat Hazards 2012;61:203–15. https://doi.org/10.1007/s11069-011-9886-5.
[7] Alvioli M, Santangelo M, Fiorucci F, Cardinali M, Marchesini I, Reichenbach P, et al. Rockfall susceptibility and network-ranked susceptibility along the Italian railway. Eng Geol 2021;293:106301. https://doi.org/10.1016/j.enggeo.2021.106301.
[8] Alvioli M, Falcone G, Mendicelli A, Mori F, Fiorucci F, Ardizzone F, et al. Seismically induced rockfall hazard from a physically based model and ground motion scenarios in Italy. Geomorphology 2023;429:108652. https://doi.org/10.1016/j.geomorph.2023.108652.
[9] di Lernia A, Buono C, Elia G. Evaluation of seismic site effects in a real slope through 2D FE numerical analyses. 9th Int. Conf. Comput. Methods Struct. Dyn. Earthq. Eng. - COMPDYN 2023, 2023:4110–24. https://doi.org/10.7712/120123.10705.20609.
[10] Falcone G, Boldini D, Amorosi A. Site response analysis of an urban area: a multi-dimensional and non-linear approach. Soil Dynam Earthq Eng 2018;109:33–45. https://doi.org/10.1016/j.soildyn.2018.02.026.
[11] Makra K, Chávez-García FJ, Raptakis D, Pitilakis K. Parametric analysis of the seismic response of a 2D sedimentary valley: implications for code implementations of complex site effects. Soil Dynam Earthq Eng 2005;25:303–15. https://doi.org/10.1016/j.soildyn.2005.02.003.
[12] Ashayeri I, Sadr A, Biglari M, Haghshenas E. Comprehensive ambient noise analyses for seismic microzonation of sarpol-e-zahab after the Mw 7.3 2017 Iran earthquake. Eng Geol 2020;272:105636. https://doi.org/10.1016/j.enggeo.2020.105636.
[13] Panzera F, Romagnoli G, Tortorici G, D'Amico S, Rizza M, Catalano S. Integrated use of ambient vibrations and geological methods for seismic microzonation. J Appl Geophys 2019;170:103820. https://doi.org/10.1016/j.jappgeo.2019.103820.
[14] Pilz M, Parolai S, Leyton F, Campos J, Zschau J. A comparison of site response techniques using earthquake data and ambient seismic noise analysis in the large urban areas of Santiago de Chile. Geophys J Int 2009;178:713–28. https://doi.org/10.1111/j.1365-246X.2009.04195.x.
[15] Dravinski M, Ding G, Wen K-L. Analysis of spectral ratios for estimating ground motion in deep basins. Bull Seismol Soc Am 1996;86:646–54. https://doi.org/10.1785/BSSA0860030646.
[16] Ibs-von Seht M, Wohlenberg J. Microtremor measurements used to map thickness of soft sediments. Bull Seismol Soc Am 1999;89:250–9. https://doi.org/10.1785/BSSA0890010250.
[17] Albarello D, Cesi C, Eulilli V, Guerrini F, Lunedei E, Paolucci E, et al. The contribution of the ambient vibration prospecting in seismic microzoning: an

example from the area damaged by the April 6, 2009 L'Aquila (Italy) earthquake. Bull GeoPhys ObServ 2011;52:513–38. https://doi.org/10.4430/bgta0013.
[18] Jiang C, Yahong D, Huangdong M, You X, Ge C. A microtremor study to reveal the dynamic response of earth fissure site: the case study in Fenwei Basins, China. Environ Earth Sci 2022 813 2022;81:1–15. https://doi.org/10.1007/S12665-022-10217-Y.
[19] Moscatelli M, Vignaroli G, Pagliaroli A, Razzano R, Avalle A, Gaudiosi I, et al. Physical stratigraphy and geotechnical properties controlling the local seismic response in explosive volcanic settings: the Stracciacappa maar (central Italy). Bull Eng Geol Environ 2021;80:179–99. https://doi.org/10.1007/s10064-020-01925-5.
[20] Oubaiche EH, Chatelain J-L, Bouguern A, Bensalem R, Machane D, Hellel M, et al. Experimental relationship between ambient vibration H/V peak amplitude and shear-wave velocity contrast. Seismol Res Lett 2012;83:1038–46. https://doi.org/10.1785/0220120004.
[21] Stanko D, Markušić S. An empirical relationship between resonance frequency, bedrock depth and VS30 for Croatia based on HVSR forward modelling. Nat Hazards 2020;103:3715–43. https://doi.org/10.1007/s11069-020-04152-z.
[22] Thabet M. Site-specific relationships between bedrock depth and HVSR fundamental resonance frequency using KiK-NET data from Japan. Pure Appl Geophys 2019;176:4809–31. https://doi.org/10.1007/S00024-019-02256-7.
[23] Vignola L, Gallipoli MR, Chiauzzi L, Stabile TA, Piscitelli S, Santarsiero G, et al. Geophysical and engineering analysis of different earthquake damage in Pescara del Tronto and Vezzano (Arquata del Tronto Municipality) following the 24th August 2016 central Italy earthquake. Bull Earthq Eng 2019;17:5471–93. https://doi.org/10.1007/s10518-018-0450-5.
[24] Castellaro S, Musinu G. Resonance versus shape of sedimentary basins. Bull Seismol Soc Am 2023;113:745–61. https://doi.org/10.1785/0120210277.
[25] Del Gaudio V, Coccia S, Wasowski J, Gallipoli MR, Mucciarelli M. Detection of directivity in seismic site response from microtremor spectral analysis. Nat Hazards Earth Syst Sci 2008;8:751–62. https://doi.org/10.5194/nhess-8-751-2008.
[26] Del Gaudio V, Muscillo S, Wasowski J. What we can learn about slope response to earthquakes from ambient noise analysis: an overview. Eng Geol 2014;182:182–200. https://doi.org/10.1016/j.enggeo.2014.05.010.
[27] Lattanzi G, Castellaro S, Di Donato M. On the time-stability of resonance frequencies in deep basins. Geophys J Int 2023;234:1870–84. https://doi.org/10.1093/gji/ggad172.
[28] Manne A, Satyam ND. Estimation of local site effects using microtremor testing in vijayawada city, India. Géotech Lett 2013;3:173–9. https://doi.org/10.1680/geolett.13.00033.
[29] Pischiutta M, Cianfarra P, Salvini F, Cara F, Vannoli P. A systematic analysis of directional site effects at stations of the Italian seismic network to test the role of local topography. Geophys J Int 2018;214:635–50. https://doi.org/10.1093/gji/ggy133.
[30] Sgattoni G, Lattanzi G, Castellaro S. An experimental approach to unravel 2D ground resonances: application to an alluvial-sedimentary basin. Earth Planets Space 2023;75:74. https://doi.org/10.1186/s40623-023-01825-4.
[31] Warnana DD, Soemitro RAA, Utama W. Application of microtremor HVSR method for assessing site effect in residual soil slope. Int J Basic Appl Sci IJBAS-IJENS 2011;11:100–5.
[32] Wood CM, Cox BR. Experimental data set of mining-induced seismicity for studies of full-scale topographic effects. Earthq Spectra 2015;31:541–64. https://doi.org/10.1193/020314EQS026.
[33] Mele M, Bersezio R, Bini A, Bruno M, Giudici M, Tantardini D. Subsurface profiling of buried valleys in central alps (northern Italy) using HVSR single-station passive seismic. J Appl Geophys 2021;193:104407. https://doi.org/10.1016/j.jappgeo.2021.104407.
[34] Pazzi V, Di Filippo M, Di Nezza M, Carlà T, Bardi F, Marini F, et al. Integrated geophysical survey in a sinkhole-prone area: microgravity, electrical resistivity tomographies, and seismic noise measurements to delimit its extension. Eng Geol 2018;243:282–93. https://doi.org/10.1016/j.enggeo.2018.07.016.
[35] Fiorucci M, Martino S, Della Seta M, Lenti L, Mancini A. Seismic response of landslides to natural and man-induced ground vibrations: evidence from the Petacciato coastal slope (central Italy). Eng Geol 2022;309:106826. https://doi.org/10.1016/j.enggeo.2022.106826.
[36] Pazzi V, Tanteri L, Bicocchi G, D'Ambrosio M, Caselli A, Fanti R. H/V measurements as an effective tool for the reliable detection of landslide slip surfaces: case studies of Castagnola (La Spezia, Italy) and Roccalbegna (Grosseto, Italy). Phys Chem Earth 2017;98:136–53. https://doi.org/10.1016/j.pce.2016.10.014.
[37] Innocenti A, Rosi A, Tofani V, Pazzi V, Gargini E, Masi EB, et al. Geophysical surveys for geotechnical model reconstruction and slope stability modelling. Remote Sens 2023;15:2159. https://doi.org/10.3390/rs15082159.
[38] Calamita G, Serlenga V, Stabile TA, Gallipoli MR, Bellanova J, Bonano M, et al. An integrated geophysical approach for urban underground characterization: the Avigliano town (southern Italy) case study. Geomat Nat Hazards Risk 2019;10:412–32. https://doi.org/10.1080/19475705.2018.1526220.
[39] Ciancimino A, Foti S, Lanzo G. Stochastic analysis of seismic ground response for site classification methods verification. Soil Dynam Earthq Eng 2018;111:169–83. https://doi.org/10.1016/j.soildyn.2018.04.006.
[40] Martelli L. Assessment of seismic bedrock in deep alluvial plains. Case studies from the emilia-romagna plain. Geosci 2021;11:297. https://doi.org/10.3390/GEOSCIENCES11070297. 2021;11:297.
[41] Mascandola C, Massa M, Barani S, Albarello D, Lovati S, Martelli L, et al. Mapping the seismic bedrock of the Po plain (Italy) through ambient-vibration monitoring. Bull Seismol Soc Am 2019;109:164–77. https://doi.org/10.1785/0120180193.
[42] Giallini S, Paolucci E, Sirianni P, Albarello D, Gaudiosi I, Polpetta F, et al. Reconstruction of a reference subsoil model for the seismic microzonation of gori (Georgia): a procedure based on principal component analysis (pca). Bull Seismol Soc Am 2021;111:1921–39. https://doi.org/10.1785/0120200341.
[43] Pagliaroli A, Moscatelli M, Raspa G, Naso G. Seismic microzonation of the central archaeological area of Rome: results and uncertainties. Bull Earthq Eng 2014;12:1405–28. https://doi.org/10.1007/s10518-013-9480-1.
[44] Diaz-Segura EG. Numerical estimation and HVSR measurements of characteristic site period of sloping terrains. Géotech Lett 2016;6. https://doi.org/10.1680/jgele.16.00009.
[45] Giallini S, Sirianni P, Pagliaroli A, Pizzi A, Mancini M, Kaiser A, et al. Reconstruction of a subsoil model for local seismic response evaluation through experimental and numerical methods: the case of the Wellington CBD, New Zealand. Eng Geol 2024;330:107413. https://doi.org/10.1016/j.enggeo.2024.107413.
[46] Falcone G, Elia G, di Lernia A. Investigating the influence of a pre-existing shear band on the seismic response of ideal step-like slopes subjected to weak motions: preliminary results. Geosciences 2023;13:148. https://doi.org/10.3390/geosciences13050148.
[47] Cotecchia V. Relazione geologica e geotecnica per la costruzione di un tratto di linea ferroviaria tra Matera e Ferrandina in funzione di collegamento diretto della Città di Matera alla rete F.S. Progetto Esecutivo. Stazione Ferrandina - Stazione di Matera la Martella; 1985.
[48] Melidoro G, Guerricchio S, Melidoro NL. Comportamento di una galleria stradale al piede di un grande corpo di frana antica. Geol Appl Idrogeol 1996;31:365–71.
[49] Falcone G, di Lernia A, Elia G. 3D modelling of construction sequences and subsoil heterogeneity effects on the seismic response of shallow tunnels in complex topographical settings. Comput Geotech 2025;180. https://doi.org/10.1016/j.compgeo.2025.107077.
[50] Bonnefoy-Claudet S, Cornou C, Bard P-Y, Cotton F, Moczo P, Kristek J, et al. H/V ratio: a tool for site effects evaluation. Results from 1-D noise simulations. Geophys J Int 2006;167:827–37. https://doi.org/10.1111/j.1365-246X.2006.03154.x.
[51] IFFI. Inventario dei fenomeni franosi. https://idrogeo.isprambiente.it/app/iffi?@=40; 2023. 511374234480854,16.477189161748353,13.
[52] Del Prete M, Giaccari E, Trisorio Liuzzi G. Rischio da frane intermittenti a cinematica lenta nelle aree montuose e collinari urbanizzate della Basilicata. CNR - GNDCI, Rapporto 1992 - U.O 1993;237:38–58.
[53] Cafaro F, Cotecchia F. Structure degradation and changes in the mechanical behaviour of a stiff clay due to weathering. Geotechnique 2001;51:441–53. https://doi.org/10.1680/GEOT.2001.51.5.441.
[54] Del Prete M, Valentini G. Le caratteristiche geotecniche delle argille azzurre dell'Italia sud-orientale in relazione alle differenti situazioni stratigrafiche e tettoniche. Geol Appl Idrogeol 1971;VI:197–215.
[55] Mucciarelli M, Gallipoli MR. A critical review of 10 years of microtremor HVSR technique. Bull GeoPhys ObServ 2001;42:255–66.
[56] Sesame WG. Guidelines for the implementation of the H/V spectral ratio technique on ambient vibrations-Measurements, processing and interpretation. 2004.
[57] Picozzi M, Parolai S, Albarello D. Statistical analysis of noise horizontal-to-vertical spectral ratios (HVSR). Bull Seismol Soc Am 2005;95:1779–86. https://doi.org/10.1785/0120040152.
[58] Loke MH, Barker RD. Rapid least-squares inversion of apparent resistivity pseudosections by a quasi-Newton method 1. Geophys Prospect 1996;44:131–52. https://doi.org/10.1111/j.1365-2478.1996.tb00142.x.
[59] Binley A, Kemna A. DC resistivity and induced polarization methods. In: Rubin Y, Hubbard SS, editors. Hydrogeophysics. Water sci. Technol. Libr., vol. 50. Dordrecht: Springer; 2005. p. 129–56. https://doi.org/10.1007/1-4020-3102-5.
[60] Brinkgreve R, Kumarswamy S, Swolfs W. PLAXIS 2D connect edition V22.1. Reference manual; 2022.
[61] Benz T, Vermeer PA, Schwab R. A small-strain overlay model. Int J Numer Anal Methods GeoMech 2009;33:25–44. https://doi.org/10.1002/nag.701.
[62] Schanz T, Vermeer PA, Bonnier PG. The hardening soil model: formulation and verification. Beyond 2000 Comput. Geotech. 1st Editio 1999:281–96.
[63] Bentivenga M, Piccarreta M. Geomorphology of pisticci area (Basilicata, southern Italy). J Maps 2016;12:220–6. https://doi.org/10.1080/17445647.2016.1193776.
[64] Viggiani G, Atkinson JH. Stiffness of fine-grained soil at very small strains. Geotechnique 1995;45:249–65. https://doi.org/10.1680/geot.1995.45.2.249.
[65] Romagnoli G, Tarquini E, Porchia A, Catalano S, Albarello D, Moscatelli M. Constraints for the vs profiles from engineering-geological qualitative characterization of shallow subsoil in seismic microzonation studies. Soil Dynam Earthq Eng 2022;161:107347. https://doi.org/10.1016/J.SOILDYN.2022.107347.
[66] Castellaro S, Mulargia F. The effect of velocity inversions on H/V. Pure. Appl Geophys 2009;166:567–92. https://doi.org/10.1007/s00024-009-0474-5.
[67] Mori F, Mendicelli A, Moscatelli M, Romagnoli G, Peronace E, Naso G. A new Vs30 map for Italy based on the seismic microzonation dataset. Eng Geol 2020;275:105745. https://doi.org/10.1016/j.enggeo.2020.105745.
[68] Molnar S, Sirohey A, Assaf J, Bard P-Y, Castellaro S, Cornou C, et al. A review of the microtremor horizontal-to-vertical spectral ratio (MHVSR) method. J Seismol 2022;26:653–85. https://doi.org/10.1007/s10950-021-10062-9.
[69] Amorosi A, Boldini D, di Lernia A. Seismic ground response at Lotung: hysteretic elasto-plastic-based 3D analyses. Soil Dynam Earthq Eng 2016;85:44–61. https://doi.org/10.1016/j.soildyn.2016.03.001.
[70] Amorosi A, Boldini D, di Lernia A. Dynamic soil-structure interaction: a three-dimensional numerical approach and its application to the Lotung case study. Comput Geotech 2017;90:34–54. https://doi.org/10.1016/j.compgeo.2017.05.016.

[71] Kuhlemeyer RL, Lysmer J. Finite element method accuracy for wave propagation problems. J Soil Mech Found Div 1973;99:421–7. https://doi.org/10.1061/JSFEAQ.0001885.
[72] Lysmer J, Kuhlemeyer RL. Finite dynamic model for infinite media. J Eng Mech Div 1969;95:859–77. https://doi.org/10.1061/JMCEA3.0001144.
[73] Régnier J, Bonilla L, Bard P, Bertrand E, Hollender F, Kawase H, et al. International benchmark on numerical simulations for 1D, nonlinear site response (PRENOLIN): verification phase based on canonical cases. Bull Seismol Soc Am 2016;106:2112–35.
[74] Régnier J, Bonilla L, Bard P, Bertrand E, Hollender F, Kawase H, et al. PRENOLIN: international benchmark on 1D nonlinear site-response analysis—validation phase exercise. Bull Seismol Soc Am 2018;108:876–900. https://doi.org/10.1785/0120170210.
[75] Clough RW, Penzien J. Dynamics of structures. Computers & structures. Berkley: Inc.; 1995.
[76] Mejia LH, Dawson EM. Earthquake deconvolution for FLAC. 4th int. FLAC symp. Numer. Model. Geomech. Minneapolis: Itasca Consulting Group; 2006.
[77] Amorosi A, Boldini D, Elia G. Parametric study on seismic ground response by finite element modelling. Comput Geotech 2010;37:515–28. https://doi.org/10.1016/j.compgeo.2010.02.005.
[78] Bathe KJ. Finite element procedures. second ed. Upper Saddle River, N.J.: Prentice Hall; 1996.